

Article

Experimental Comparison of Three Real-Time Optimization Strategies Applied to Renewable/FC-Based Hybrid Power Systems Based on Load-Following Control

Nicu Bizon ^{1,2,*}  and Mihai Oproescu ¹

¹ Faculty of Electronics, Communications and Computers Science, University of Pitesti, 110040 Pitesti, Romania; mihai.oproescu@upit.ro

² Doctoral School, University Politehnica of Bucharest, 061071 Bucharest, Romania

* Correspondence: nicu.bizon@upit.ro

Received: 19 November 2018; Accepted: 17 December 2018; Published: 19 December 2018



Abstract: Besides three different real-time optimization strategies analyzed for the Renewable/Fuel Cell Hybrid Power Systems (REW/FC-HPS) based on load-following (LFW) control, a short but critical assessment of the Real-Time Optimization (RTO) strategies is presented in this paper. The advantage of power flow balance on the DC bus through the FC net power generated using the LFW control instead of using the batteries' stack is highlighted in this study. As LFW control consequence, the battery operates in charge-sustained mode and many advantages can be exploited in practice such as: reducing the size of the battery and maintenance cost, canceling the monitoring condition of the battery state-of-charge etc. The optimization of three FC-HPSs topologies based on appropriate RTO strategy is performed here using indicators such as fuel economy, fuel consumption efficiency, and FC electrical efficiency. The challenging task to optimize operation of the FC-HPS under unknown profile of the load demand is approached using an optimization function based on linear mix of the FC net power and the fuel consumption through the weighting coefficients k_{net} and k_{fuel} . If optimum values are chosen, then a RTO switching strategy can improve even further the fuel economy over the entire range of load.

Keywords: fuel cell system; fuel economy; hybrid power systems; unknown load demand; real-time optimization; control loops switching strategy

1. Introduction

In renewable energy Hybrid Power Systems (HPS) applications, the generation power is usually intermittent and variable, the load power is also dynamic with the daily energy consumption, such as in Fuel Cell Hybrid Power Systems (FC-HPS), wind turbine farms, and solar arrays.

The main objective for the FC-HPS [1–4] and other hybrid energy systems [5–7] is to efficiently operate these systems based on rule-based and optimization-based strategies proposed in the last years [8,9]. As it is known, the deterministic rule-based strategy is already available in the market due to their reduced complexity in implementation, but this type of strategy cannot find the optimum solution [10], so the research interest has switched to optimization-based Real-Time Optimization (RTO) strategies, even if the complexity increases [1,11]. These strategies can find and track in real-time the optimal solution or a suboptimal solution close to it [7,12]. The RTO strategies usually use optimization algorithms such as the Extremum Seeking (ES) algorithms [13,14], the Equivalent Consumption Minimization Strategy (ECMS) [15,16], the intelligent algorithms [17–19], the Model Predictive Control (MPC) schemes [20,21], and so on [22–26]. From these RTO-strategies, the ECMSs

based on Pontryagin's Minimum Principle (PMP) [26,27] or Dynamic Programming (DP) are most used for FC-HPS [10].

Different ES-based RTO strategies based on classical [28,29], modified [30,31], and advanced [13,14,32,33] ES algorithms were proposed recently to optimally operate the FC-HPS. The modified ES algorithm improves the tracking robustness compared to conventional ES algorithm due to the use of a Band-Pass Filter (BPF) to process more power harmonics into the seeking signal [30,31]. The advanced ES algorithm improves the tracking accuracy compared to modified ES algorithm by using modulation of the dither amplitude with the magnitude of first harmonics of the FC power. Furthermore, the FC ripple power decreases around the Maximum Efficiency Point (MEP), which is faster found [32]. A comparative study of the ES-based RTO strategies is presented in [33,34]. The global ES (GES) algorithm tracks the global Maximum Power Point (MPP) instead of local MPP, improving with more than 30% the efficiency of the photovoltaic (PV) system [35–37]. The GES algorithm [35] uses two BPFs instead of one BPF [36]. The design rules for the GES algorithms are detailed in [37].

PV arrays, wind turbines and battery stacks generate the needed load power in renewable energy systems and a design to comply the power flow balance on the Direct Current (DC) bus could oversize the battery stack due to the high dynamics of the load profile and variability of the available renewable energy. This issue can be solved by using the Load-Following (LFW) control of the FC boost converter [38] to compensate the power flow balance on the DC and the battery will operate in charge sustaining mode, which means reducing the size of the batteries stack. Thus, considering additionally the reduction of maintenance costs, the overall cost of FC-HPS remains within the same range as the battery-based HPS cost. Furthermore, for example, the LFW control is simpler to be implemented compared to ES-based RTO routine to rescale the air flow rate (*AirFr*) of the Proton Exchange Membrane FC (PEMFC) system or other energy management strategies based on states' diagram [39]. Different RTO-strategies have been proposed for FC-HPS to improve the free air breathing of PEMFC system through the MEP [40] or MPP [41] tracking techniques, or based on other robust control techniques [42] which are analyzed and compared in [43]. The MPP tracking technique improves the tracking accuracy of a photovoltaic/FC-HPS by simultaneously optimizing both the PV and FC systems [44]. The renewable HPS architecture requires a FC system and electrolyzer to store the hydrogen in order to mitigate the variability of the renewable power, but a regenerative FC stack could solve this issue in one device [45,46].

Besides the LFW control of the FC system [38], other different algorithms can be used as well [46], such as artificial intelligent algorithms [47] based on neural networks [48], genetic algorithms [49], or data fusion approach [50]. The combinatorial techniques [51], the Model Reference Adaptive Control (MRAC) [52], the metaheuristic approaches [53], the prediction of the load demand [54], and ECMSs techniques [55] are other methods proposed to optimize the operation of the FC-HPS.

The static feed-forward (sFF) control of the FC system was first implemented in practice [56], but many other control algorithms for air compressor systems have been designed based on the Hardware-in-Loop System (HILS) technique [56–67]. The HILS-based second order sliding mode controller implemented in a commercial twin screw air compressor sub-optimally controls the air feed system [57] avoiding oxygen starvation and the compressor surge phenomenon using the load governor method and constrained extremum technique [58]. Thus, the *AirFr* of the PEMFC system can be optimally control by a second order sliding mode control [59]. The better mitigation of load ripples and pulses on PEMFC operation can be ensured using a disturbance rejection control [60] or a differential flatness approach [61] compared to a classic Proportional–Integral (PI) controller [56]. Also, by appropriate control of the cathode system, the lifetime of the PEMFC system could be increased to 25 years in next decade [62]. The Linear Quadratic Regulator (LQR)/Linear Quadratic Gaussian (LQG) control maintains the best oxygen stoichiometry in PEMFC systems [63], but other optimal control solutions for the *AirFr* are proposed in literature based on ES algorithm [32], feed-forward

fuzzy Proportional Integral Derivative (PID) control [64], optimal PID plus fuzzy controller [65], time delay control [66], and adaptive control [67].

Besides control for air systems, other control solutions to improve the fuel economy of the fuel system were proposed [43] such as global optimization methods based on fuzzy logic [68] and genetic [49] algorithms, adaptive algorithms such as adaptive fuzzy control [69] and adaptive Energy Management Strategy (EMS) [70], but most of them require prior knowledge of the driving cycle. Furthermore, these algorithms are difficult to implement in RTO strategies due to its computational complexity; so, the research field of designing efficient and simple RTO strategies for FC-HPS still remains challenging.

In this paper, using Matlab-Simulink version 2013[®], the performance of three LFW control-based FC-HPS topologies is compared considering the optimization loop implemented to size the FC boost converter (the new RTO3 strategy), *AirFr* regulator (the RTO2 strategy [71]), or Fuel Flow rate (*FuelFr*) regulator (the RTO1 strategy [72]). All the topologies use one optimization loop and LFW control to mitigate the variability of the load demand and renewable energy on battery State-Of-Charge (SOC). The performance of the proposed RTO strategies is compared to the sFF reference strategy under same unknown profile of the Load Cycle (LC) based on the following indicators: (1) the FC net power, (2) the fuel consumption efficiency, (3) the electrical efficiency of the FC system, and (4) the total fuel consumption. The optimization function used in this study is designed to reduce the total fuel consumption under unknown LC, being a linear weighted function of the FC energy efficiency and the fuel consumption efficiency through the weighting coefficients k_{net} and k_{fuel} . The GES algorithm is used to find in real-time the global maximum of the optimization function [35].

Design of the weighting coefficients k_{net} and k_{fuel} will improve the fuel economy of a FC vehicle under unknown LC. Thus, the performance is estimated for all three FC-HPS topologies compared to the sFF strategy using same profile for the constant and variable load demand. The RTO strategies for the FC-HPS topologies clearly differ in the place where the optimization is performed and the LFW control is applied (see Table 1). Finally, considering the obtained performance, some guiding design rules to choose the switching RTO strategy are given.

The paper is organized as follows: optimization objectives and algorithms for FC-HPS based on the extremum seeking algorithm are very briefly mentioned in Section 2. The LFW control-based RTO strategies with specific optimization loop are designed in Section 3 considering the power flow balance at the DC bus. The results for all three RTO strategies are presented in Section 4 compared to the sFF strategy for constant and variable load, without and with renewable energy support. Section 5 discusses the results obtained and the last section concludes the paper.

2. Optimization Objectives and Algorithms

The RTO switching control strategies proposed in this paper will be implemented based on the theory of problem optimization applied in many engineering applications.

2.1. Optimization Algorithms

Optimization of the FC-HPS is the real-time process of searching for the set of values in the search range, called the optimal value (or the optimum) and which must be very close to the global extreme of the optimization function, so besides high tracking and searching accuracy [35,36], the global search feature of the optimization algorithm must have a 100% hit count and to have a good robustness to different perturbations into the system (such variations of the load demand and renewable power) [5,6,73]. The input vector will continuously seek the new optimum in the searching range due to changes in the requested load demand and available renewable power which set the needed FC power under LFW control. If some stationary regimes could appear, then the FC ripple current must be minimum [35,36,74]. The FC net power $P_{FCnet} = f(AirFf, FuelFr)$ has an optimum called MEP and many other peaks on the plateau around the MEP [1], but 99.9% searching accuracy and less than 1% searching resolution help the GES algorithm to discern the MEP from them [37], so the

ES algorithm [37] was used in this study due to its reported performance features and location and tracking of the MEP in one search stage (less than 10 dither periods, which, for example, means less than 0.01 s for a 1000 Hz sinusoidal dither). The firmware-based global MPP tracking algorithms proposed in literature operate in two stages, so their tracking time results are higher compared to the GES algorithm. The tracking accuracy (T_{acc}) and searching resolution (S_R) are defined as follows [37]:

$$S_R = \frac{\min_i |y_{GMPP} - y_{LMPPi}|}{y_{GMPP}} \cdot 100[\%] \quad (1)$$

$$T_{acc} = \frac{y_{GMPP}^*}{y_{GMPP}} \cdot 100[\%] \quad (2)$$

where y_{GMPP} , $y_{LMPP} < y_{GMPP}$, and $y_{GMPP}^* < y_{GMPP}$ are the global extreme, the local maxima, and the value tracked with the GMPPT algorithm.

Furthermore, the GES algorithm [37] does not need complicated and periodic tuning of the parameters [75], so it is simple to design and implement [76], but ultimately the performance of all optimization algorithms depend on the to optimization objectives and constraints defined for a specific FC-HPS.

2.2. Optimization Objectives and Constraints

The optimization procedure usually follows the following steps: identifying and defining the optimization problem, designing the model, simulating and evaluating the model, refine the problem, and finally implementing optimal solution. The optimization objectives are in general contradictory, so multi optimization functions are proposed instead of one optimization function [77], integrating the constraints by penalty function related to battery SOC level [78,79].

The FC-HPS optimization can be generally defined as follows:

Maximize:

$$f(x, AirFr, FuelFr, P_{Load}) = k_{net} \cdot P_{FCnet} + k_{fuel} \cdot Fuel_{eff} \quad (3a)$$

Subject to FC-HPS dynamics:

$$\dot{x} = g(x, AirFr, FuelFr, P_{Load}), x \in X \quad (3b)$$

and battery SOC constraints:

$$SOC_{min} < SOC < SOC_{max} \quad (3c)$$

In Equations (3a–c) P_{Load} , k_{net} and k_{fuel} represent the disturbance input, respectively weighting coefficients that will be switched according to the objectives defined in real-time during an unknown LC [80].

For example, the FC vehicle will adapt the parameters of the used optimization function considering the available on-line information about the route profile or the requests from as inputs of the Energy Management Unit (EMU) [81,82] as follows: the FC net power must be maximized if the FC vehicle climbs up a hill, the fuel economy must be maximized if the FC vehicle runs smoothly on the highway, the fuel consumption efficiency must be maximized if the communication unit informs the EMU that the fuel tank is almost empty based on signaling sensors, but a fuel station is close to the current position of the FC vehicle.

The number of sensors must be reduced at minimum for the FC-HPS based on Renewable Energy Systems (RES) by using adaptive algorithms to improve the fuel economy for plug-in FC vehicles [83] or grid-connected FC-HPS [84], which usually use many decision variables and constraints as inputs for the EMU such as [85]: the number of energy source units (FC systems, PV panels, wind turbines (WT), batteries, power storage devices, electrolyzers), RES potential (insolation and wind speed in installation area), technical characteristics (PV panel position, WT height), battery

characteristics (SOC_{min} , SOC_{max}), hydrogen storage availabilities (tank volume, electrolyzer capacity), type of power storage devices (superconducting magnetic energy storage or SMES, flywheel energy storage or FES, ultracapacitors) and so on [1,4]. The constraints to design the FC-HPS of a FC vehicle are clearly related to available space and weight limitations, lifetime and safe operation of the FC system and batteries stack, maintenance cost, and so on [83], so an optimization problem involving multiple objectives such as technical, economic, and environmental objectives must be a combination of the conflicting performance indicators to be easy implemented [1,45]. Besides the fuel economy (or total fuel consumption: $Fuel_T = \int FuelFr(t)dt$) as general performance indicator, other performance indicators can be integrated in the optimization function depending of application and load profile [86], but also by the environment conditions due to emplacement of the FC-HPS in different places situated on worldwide [87]. For example, fuel economy, lithium battery size and powertrain system durability, and, respectively, fuel economy and power efficiency are linearly mixed in the optimization function used in [88,89]. The performance indicators that could be used are as follows: the fuel consumption efficiency ($Fuel_{eff} = \frac{P_{FCnet}}{FuelFr}$), the FC electrical efficiency ($\eta_{sys} = \frac{P_{FCnet}}{P_{FC}}$), and the efficiency of hydrogen consumption ($eff_{H_2} = \frac{100 \times P_{FCnet}}{LHV \times Fuel_T}$), where LHV is the lower heating value for hydrogen fuel. The range for indicator η_{sys} is between 85% (at rated load) to 90% (at light load) and for indicator eff_{H_2} is up to 60%, but these performances could be improved [90].

The power loss from the FC stack power (P_{FC}) to supply the air compressor (P_{cm}) represents about 10–15%, so the available FC net power in the power flow balance on the DC bus will be $P_{FCnet} \cong P_{FC} - P_{cm}$, where $P_{cm} = I_{cm} \times V_{cm} = a_1 \times AirFr^2 + a_2 \times AirFr + a_3 \times (b_1 \times I_{FC} + b_0)$, and $a_3 = 0.6$, $a_2 = 0.04$, $a_1 = -0.00003231$, $b_0 = 0.9987$, and $b_1 = 46.02$ [29].

This research study is motivated by the complexity of implementation for all control strategies studied in the literature until now, so, in this paper, three different FC-HPSs topologies have been analyzed considering the same operating conditions (load demand profiles), optimization function, constraints (the FC current slope of 100A/s used in [91]), and GES algorithm to track the MEP in real-time. The GES algorithm and other ES control algorithms proposed in the literature will be briefly presented in the next section.

2.3. Extremum Seeking Control Algorithm

A nonlinear system can be defined by (4) [92]:

$$\dot{x} \triangleq \frac{dx}{dt} = f(x(t), u(t)), \quad y = h(x(t)) \quad (4)$$

where the smooth functions $f(x,u)$, $h(x)$, and $u(t) = g(x(t),p)$ define the system dynamic, nonlinear map of the system, and the control law, $x \in R^n$, $u \in R^m$, and $y \in R$ are the state variables, system inputs and system output, and p is the parameter vector.

The nonlinear system evolves under ES control to the equilibrium point (the optimum) defined by the smooth function $x_e, x_e:R^l \rightarrow R^n$:

$$f(x, g(x, p)) = 0 \quad \Leftrightarrow \quad x = x_e(p) \quad (5)$$

and the parameter-output map:

$$y = h(x) = h(x_e(p)) = h(p) \quad (6)$$

based on the seeking vector p .

The Asymptotic Perturbed Extremum Seeking Control (aPESC) scheme based on Scalar PESC (PESCs) scheme [92] was proposed in [93] (see Figure 1a with the switch on position 1). The tuning parameters k_1 and k_2 change the amplitude of the tracking signal (\hat{p}_1) and the sweeping signal (\hat{p}_2). Due to some stability issues of the tracking loop of the PESCs scheme, in general the tuning parameter k_2 cannot be increased to scan the entire search range, so the sweeping signal \hat{p}_2 in aPESC scheme must

be a modulated signal (the dither modulated with the dither gain G_d ; see Figure 1a with the switch on the position 2) to increase the sweeping range due to dither gain G_d which decreases asymptotically exponentially from a high initial value (a_0) to zero based on function q . Thus, the convergence of this method depends to starting point, the value a_0 , and function q , so initial assumptions mentioned in [92] must to be complied to find the optimum in all cases. The aPESC scheme based on the Lyapunov function (see the aPESCLy scheme in Figure 1b with the switch on position 1) tries to improve the convergence by using a sweeping signal \hat{p}_2 which is maintained to high value a_0 until the optimum is located. Then, the sweeping signal \hat{p}_2 decreases to zero based on dither gain G_d which evolves exponentially to zero, ensuring the stability of the tracking loop. The performance of the aPESCLy scheme depends on quite complicated design of the Lyapunov function (which uses three signals from the tracking loop and a switching threshold), and parameters a_0 and ρ [94]. The convergence of the aPESCH1 scheme is improved compared to aPESC scheme by using a sweeping signal \hat{p}_2 based on the first harmonic (H1) of the output signal y , which define the dither gain G_d (see the aPESCH1 scheme in Figure 1b with the switch on position 2). The harmonic H1 is estimated using the Fast Fourier Transform (FFT) and its value evolves from initial high value to zero during the MEP searching. So, the entire searching range will be scanned considering the high initial gain obtained in the tracking loop by adaptive modulation of the tuning parameter k_2 [30]. The aPESCH1 scheme has features of a Global aPESC (GaPESC) scheme [35] (see GaPESCH1 scheme in Figure 1c with the switch on position 3). Consequently, the performance of this scheme is compared with other GaPESC schemes as the GaPESC scheme using one BPF (BPF1), the GaPESCbpf scheme using two BPFs (BPF1 and BPF2), and the GaPESCd scheme based on derivative operator (all these schemes are presented in Figure 1c considering the switch on position 1, 2, and 4, respectively) [36]. The minor differences between these schemes are given by the used technique (to approximate the first harmonic H1 and lets other harmonics in the tracking loop to ensure the dither persistence) as follows [37]: the BPF2 will approximate the first harmonic H1 in the GaPESCbpf scheme and the BPF1 must be designed to ensure harmonics in the tracking loop. This scheme will be used in this study and called here as the GES scheme. The tracking speed of the GaPESC scheme is lower than that of the GES scheme due to the use of a single BPF1, which must be centered on first harmonic H1. In general, the derivation operation produces instabilities in the tracking, so the GaPESCd scheme is not recommended in practice. It is worth to mention that the tracking loop is the same for all aPESC schemes analyzed in this paper or other ES schemes proposed in the literature such as the Fractional-Order ES scheme [95].

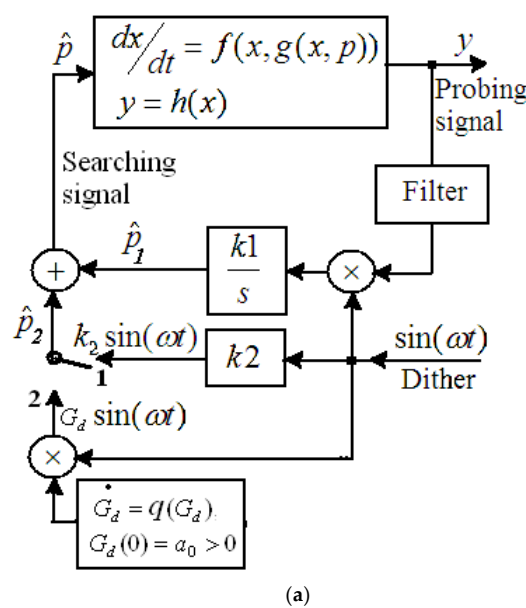
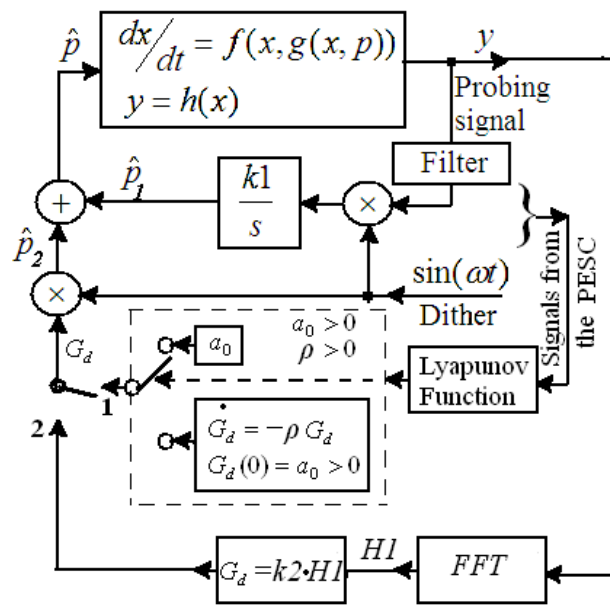
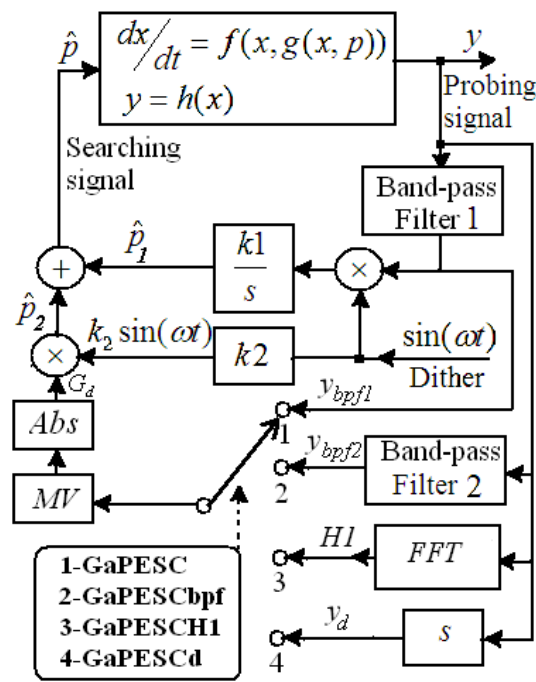


Figure 1. Cont.



(b)



(c)

Figure 1. aPESC, modified aPESC and Global aPESC schemes. (a) The scalar PESC (PESCs) scheme and its asymptotic variant (aPESCs) with the switch on the position 1 and 2; (b) Modified aPESC schemes. The aPESC schemes based on the Lyapunov function (aPESCLyy) and the H1 harmonic (aPESCH1) with the switch on the position 1 and 2; (c) Global aPESC (GaPESC) schemes.

The optimization loop is based on one or two GES control blocks (see Figure 2) implementing the relationships (7) [37]:

$$y = f(v_1, v_2), y_N = k_{Ny} \cdot y \tag{7a}$$

$$\dot{y}_f = -\omega_h \cdot y_f + \omega_h \cdot y_N, y_{HPF} = y_N - y_f, \dot{y}_{BPF} = -\omega_l \cdot y_{BPF} + \omega_l \cdot y_{HPF} \tag{7b}$$

$$y_{DM} = y_{BPF} \cdot s_d, s_d = \sin(\omega t), \tag{7c}$$

$$\dot{y}_{Int} = y_{DM} \tag{7d}$$

$$G_d = |y_{MV}|, y_{MV} = \frac{1}{T_d} \cdot \int y_{BPF} dt \tag{7e}$$

$$y_M = G_d \tag{7f}$$

$$\hat{p}_1 = k_1 \cdot y_{Int}, k_1 = \gamma_{sd} \cdot \omega \tag{7g}$$

$$\hat{p}_2 = k_2 \cdot y_M \cdot s_d \tag{7h}$$

$$\hat{p}_3 = A_m \cdot s_d \tag{7i}$$

$$I_{refGES} = k_{Np} \cdot (\hat{p}_1 + \hat{p}_2 + \hat{p}_3), \tag{7j}$$

The relationships (7a) represent the optimization function and the input normalization gain (k_{Ny}). The Equation (7b) represent the high-pass filter (HPF), respectively the band-pass filter (BPF) used to signal processing the process's output under optimization (the FC power in this case). The demodulation, the integration, the computing of the dither gain G_d based on average value (AV) of the y_{bpf} signal, and the signal that will modulate the dither are represented by the relationships (7c) to (7f). It is worth to mention that the searching signal (p) has three components that evolves different in the searching of the optimum, the tracking signal (\hat{p}_1), the sweeping signal (\hat{p}_2), and the starting minimum signal (\hat{p}_3), which are estimated based on (7g) to (7i). These components finally define the reference current I_{refGES} (6j), where the parameter k_{Np} represents the output normalization gain. Based on design rules [75], the tuning parameters are set to $k_1 = 1$ and $k_2 = 2$, and the normalization gains to $k_{Ny} = 1/Y_{Max}$ and $k_{Np} = I_{FC(rated)}/2$. In this case, the nominal value of the FC current are $I_{FC(rated)}$ and the maximum value of the optimization function are Y_{Max} . These values ensure 100% hit count for searching process [96]. The parameters of the dither frequency f_d for the two GES controllers are of 100 Hz and 200 Hz to ensure the dither persistency and separate search of optimum on optimization surface, and the BPF cut-off frequencies are defined by $b_h f_d$ and $b_1 f_d$ (where $b_h = 0.1$ and $b_h = 3.5$) [75].

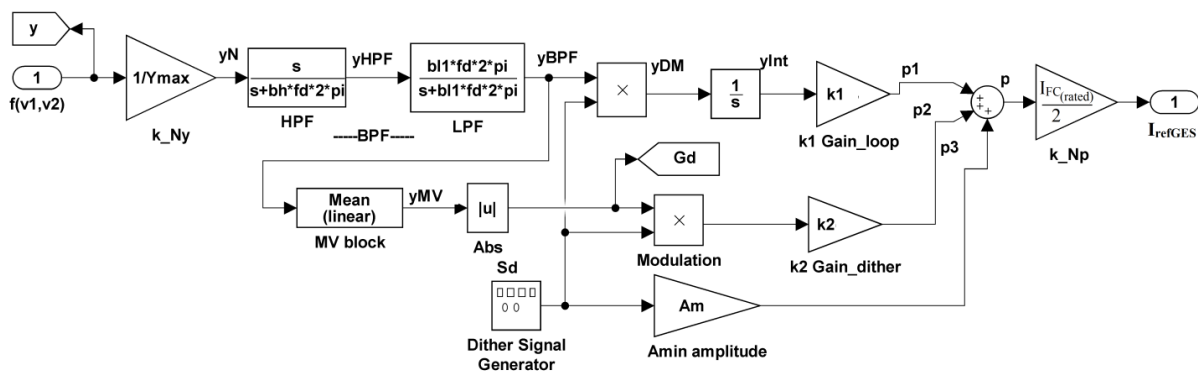


Figure 2. The GES scheme.

The searching (or tracking) time for all GES schemes discussed above are less than 10 periods of dithers [75,76], so it is less than 0.1 seconds, assuring in real time the optimal operation of the FC-HPS. The outputs of two GES controllers, $I_{ref(GES1)}$ and $I_{ref(GES2)}$, and the output of the LFW controller $I_{ref(LFW)}$ are proposed as control variable for the FC-HPS and will be presented in next section.

3. Energy Management Strategies for the Renewable Fuel Cell Hybrid Power Systems

The FC-HPS based on Renewable Energy Sources (RES block in Figure 3—top) and the EMU (Figure 3—bottom) are presented in Figure 3. The output of the LFW controller, $I_{ref(LFW)}$, will be estimated based on power flow balance on DC bus (8):

$$C_{DC} \cdot u_{dc} \cdot du_{dc} / dt = p_{DC} + p_{ESS} - p_{DCreq} \tag{8}$$

where the capacitor C_{DC} filters the voltage on DC bus (u_{dc}). The p_{DC} , p_{ESS} and p_{DCreq} , represent the output power of the boost converter, the power of Energy Storage System (ESS), respectively the power required from the FC system, on DC bus, via the boost converter:

$$p_{DCreq} = p_{Load} - p_{RES} \quad (9)$$

The output power of the FC boost converter is:

$$p_{DC} = \eta_{boost} \cdot p_{FCnet} \quad (10)$$

where $\eta_{boost} \cong 95\%$ represents the efficiency of the boost converter.

Thus, the average value (AV) of the power flow balance (8) will be given by (11):

$$0 = \eta_{boost} P_{FCnet(AV)} + P_{ESS(AV)} - P_{DCreq(AV)} \quad (11)$$

When the battery works in mode “charge-sustaining”:

$$P_{ESS(AV)} \cong 0 \quad (12)$$

then LFW reference will be given by (13):

$$I_{ref(LFW)} \cong I_{FC(AV)} = P_{DCreq(AV)} / (V_{FCnet(AV)} \eta_{boost}) \quad (13)$$

where the power requested on DC bus is the load demand from DC loads and AC loads via the inverter systems minus the available RES power:

$$p_{DC} \cong p_{DCreq} = p_{Load} - p_{RES} \Rightarrow P_{DCreq(AV)} \cong P_{Load(AV)} - P_{RES(AV)} \quad (14)$$

The inputs of the boost controller ($I_{ref(boost)}$), the air regulator ($I_{ref(Air)}$), and the fuel regulator ($I_{ref(Fuel)}$) will be controlled by the GES references based on RTO strategies setting (see Figure 4 and Table 1), as follows: the RTO1 strategy uses $I_{ref(boost)} = I_{ref(LFW)}$, $I_{ref(Fuel)} = I_{refGES} + I_{FC}$ and $I_{ref(Air)} = I_{FC}$, the RTO2 strategy uses $I_{ref(boost)} = I_{ref(LFW)}$, $I_{ref(Air)} = I_{refGES2} + I_{FC}$ and $I_{ref(Fuel)} = I_{FC}$ (both strategies being tested in [97,98] for the FC-HPS without support from the RES), and the RTO3 strategy uses $I_{ref(boost)} = I_{refGES}$, $I_{ref(Fuel)} = I_{FC}$ and $I_{ref(Air)} = I_{ref(LFW)}$ (being tested in [84,99] for the FC-HPS without support from the RES).

The FC current will follow $I_{ref(LFW)}$ for the RTO1 and RTO2 strategies due to hysteretic control of the boost converter:

$$I_{FC(AV)} \cong P_{DCreq(AV)} / (V_{FCnet(AV)} \eta_{boost}) \quad (15)$$

Consequently, the FC net power generated will be given by (16):

$$P_{FC(AV)} = I_{FC(AV)} \cdot V_{FCnet(AV)} \cong P_{DCreq(AV)} / \eta_{boost} \quad (16)$$

Thus, considering (12), $P_{ESS(AV)} \cong 0$, the LFW control is implemented using (13). The smooth value of the load demand and the FC voltage can be obtained using the AV techniques or other filtering techniques as well [100,101]. So, a smooth value will be obtained for the reference $I_{ref(LFW)}$ and the FC system will be safe operated even under sharp dynamic profiles of the load demand and RES power.

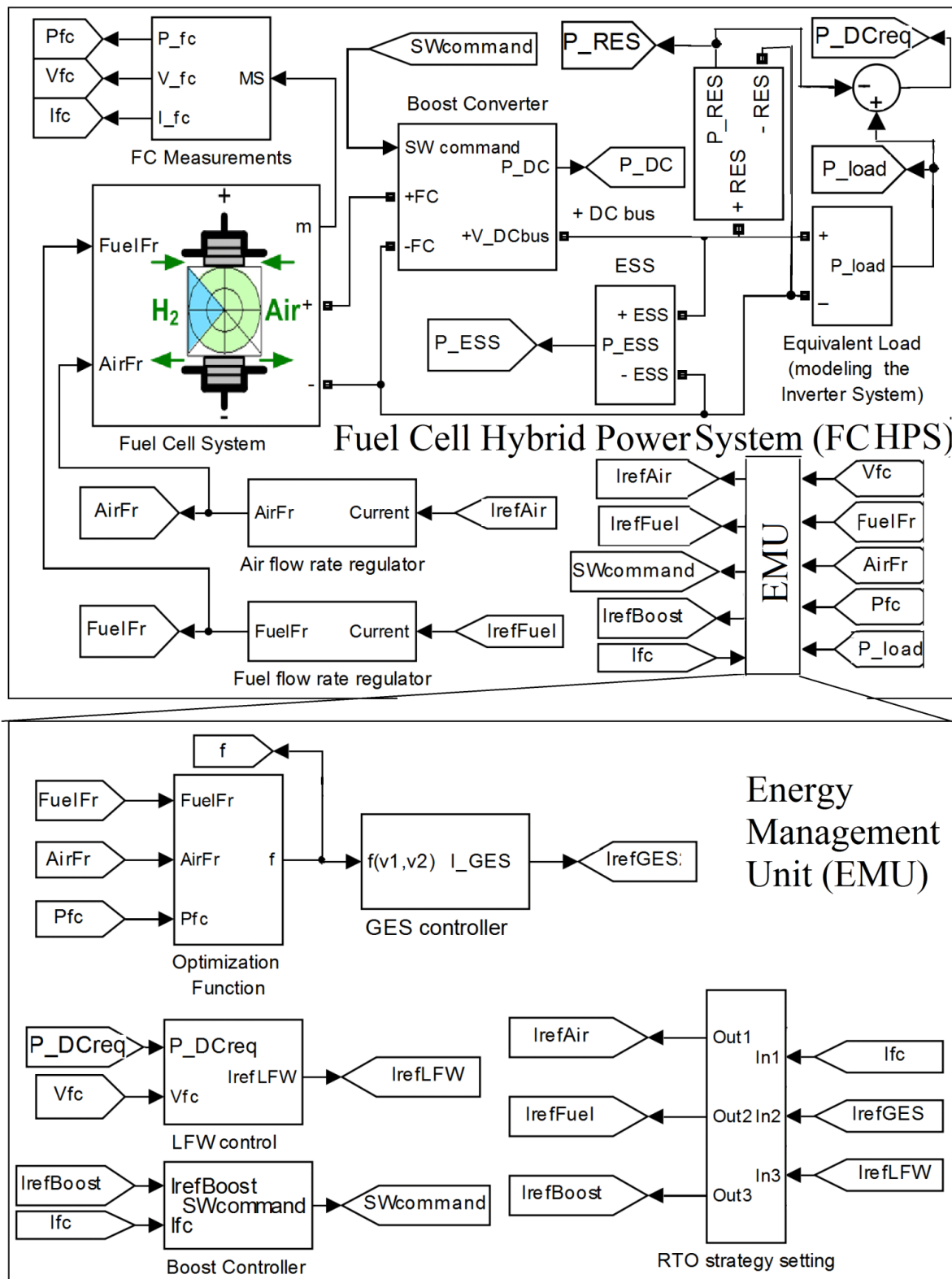


Figure 3. The FC HPS and EMU.

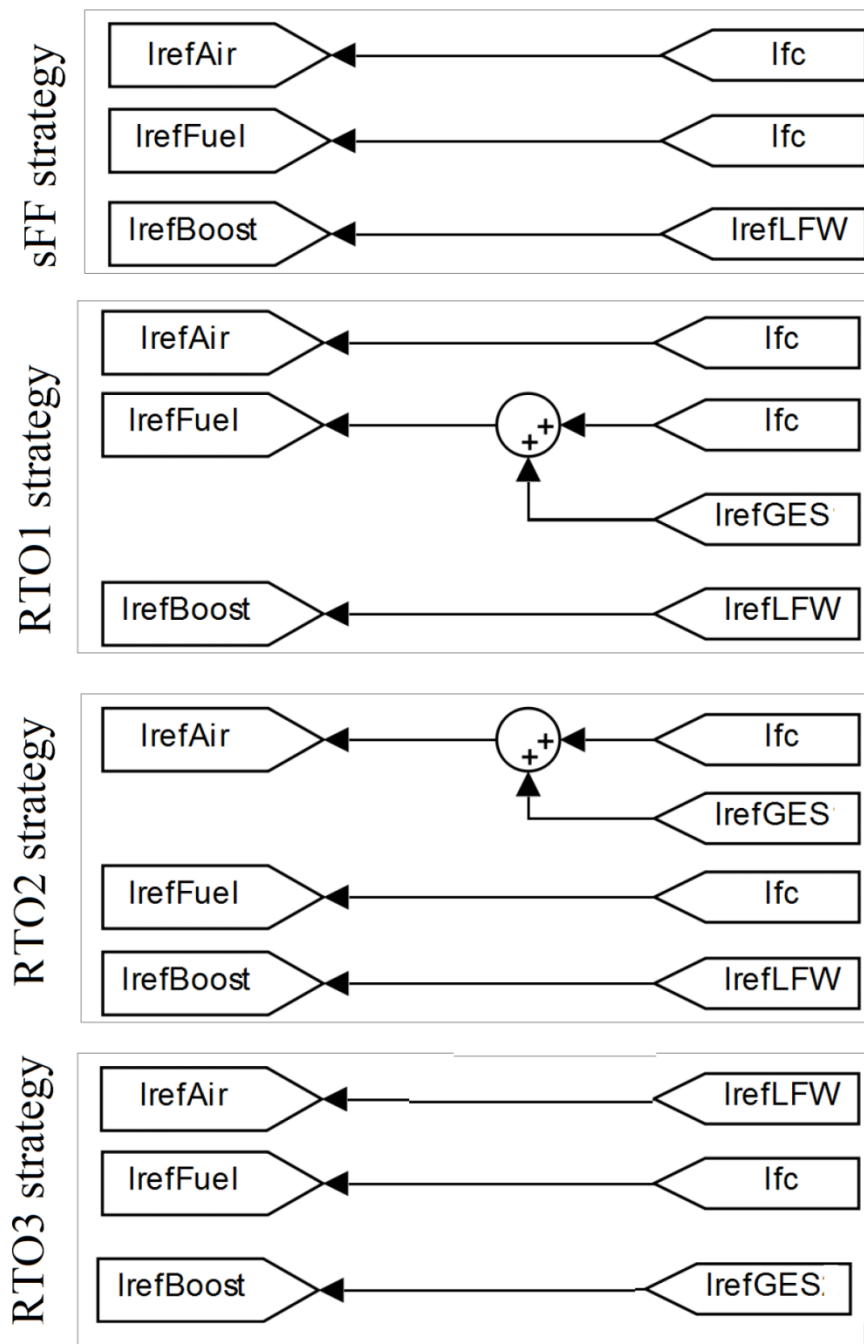


Figure 4. RTO strategy setting block.

Table 1. RTO strategies setting.

No.	$I_{ref(Boost)}$	$I_{ref(Air)}$	$I_{ref(Fuel)}$	Strategy	Reference
0	I_{LFW}	I_{FC}	I_{FC}	sFF	[56]
1	I_{LFW}	I_{FC}	$I_{GES1} + I_{FC}$	RTO1	[97]
2	I_{LFW}	$I_{GES1} + I_{FC}$	I_{FC}	RTO2	[98]
3	I_{GES2}	I_{LFW}	I_{FC}	RTO3	[84]

The references $I_{ref(Fuel)}$ and $I_{ref(Air)}$ will define the inputs $FuelFr$ and $AirFr$ of the FC system based on the fueling regulators (17) [56]:

$$FuelFr = \frac{60000 \cdot R \cdot (273 + \theta) \cdot N_C \cdot I_{ref(Fuel)}}{2F \cdot (101325 \cdot P_{f(H_2)}) \cdot (U_{f(H_2)}/100) \cdot (x_{H_2}/100)} \quad (17a)$$

$$AirFr = \frac{60000 \cdot R \cdot (273 + \theta) \cdot N_C \cdot I_{ref(Air)}}{4F \cdot (101325 \cdot P_{f(O_2)}) \cdot (U_{f(O_2)}/100) \cdot (y_{O_2}/100)} \quad (17b)$$

where R and F the constants 8.3145 J/(mol K) and 96485 As/mol, and the parameters (N_C , θ , $U_{f(H_2)}$, $U_{f(O_2)}$, $P_{f(H_2)}$, $P_{f(O_2)}$, x_{H_2} , y_{O_2}) are defined in [56].

The air and fuel regulators use 100 A/s slope limiters for safe operation of the FC-HPS [102].

Note that due to LFW control of the FC system via the boost controller, the batteries will operate in charge sustaining mode for all RTO strategies analyzed in this paper. The advantages are related to battery size, its lifetime and maintenance cost, and simple implementation of the EMU (the constraints (3c) for the battery SOC are clearly respected).

The sFF strategy proposed in [56] will be used as reference with the LFW control implemented in the same manner (see Table 1) for a fair comparison of each strategy RTO_k , $k = 1 \div 7$, based on the gaps (18) in the performance indicators:

$$\Delta\eta_{sys} = \eta_{sysk} - \eta_{sys0} \quad (18a)$$

$$\Delta Fuel_{eff} = Fuel_{effk} - Fuel_{eff0} \quad (18b)$$

$$\Delta Fuel_T = Fuel_{Tk} - Fuel_{T0} \quad (18c)$$

A PEMFC Matlab Simulink model with parameters: 6 kW/45 V is used in this study. For this model, the constant time is put to 0.1 s value. The variable voltage of FC (V_{FC}) is raised to 200 V by using a boost converter $VDC \cong VDC(ref) = 200$ V. The control type used for the boost converter is of hysteretic type with 0.1 A hysteresis band.

Similar to [103], to mitigate the pulses on the DC bus a ESS semi-active topology is chosen. This topology has a battery stack connected on DC bus (lithium-ion batteries with 100 Ah/100 V) and an ultracapacitors' stack with nominal capacity of 100 F. For this ultracapacitors' stack we have the following typical values: ESR—the equivalent series resistor—the value is 0.1 Ω , EPR—the parallel resistor—the value is 10 k Ω , and the initial voltage are set on 100 V, so to connect the ultracapacitors' stack to the DC bus, is used a bidirectional DC-DC converter. For all other model parameters, the values are the set by default. Also, the initial battery stack SOC is 80%. Both stacks use models from Matlab and Simulink® (R2013a, MathWorks, Natick, MA, USA) toolboxes (with the outputs that are offered by each model, such as SOC signal for the battery's model, and which all are explained in the help page). Furthermore, to filter the voltage on DC bus, a capacitor, C_{DC} , with 100 μ F is used (the initial value of $V_{DC} = 200$ V) [103].

4. Results

The GES-based RTO strategies will search the optimum of the optimization function (3a) for three sets of the k_{net} and k_{fuel} values (weighting coefficients): in the first situation, A, we have the following values for coefficients: $k_{net} = 0.5$, $k_{fuel} = 0$, for the second situation, B, we have the following values for coefficients: $k_{net} = 0.5$, $k_{fuel} = 25$, and for the third situation, C, the values for coefficients are: $k_{net} = 0.5$, $k_{fuel} = 50$. Different scenarios were performed in this analysis. These scenarios have taken into account the power flow over the DC bus: the load demand has been both, variable and constant, also having or not having the power of RES.

4.1. HPS under Constant Load Demand and $k_{fuel} = 0$ and $P_{RES} = 0$

The value of the performance indicators η_{sys0} , $Fuel_{eff0}$, and $Fuel_{T0}$ for the sFF strategy are presented in [71].

FC Electrical Efficiency

Results such as deficiencies in fuel economy, fuel efficiency, and global fuel efficiency are presented in Tables 2–4 for each strategy $RTOk$, $k = 1 \div 3$, compared to sFF strategy in case A ($k_{fuel} = 0$) under constant load.

Table 2. The gaps in FC electric efficiency.

P_{load}	$\Delta\eta_{sys1}$	$\Delta\eta_{sys2}$	$\Delta\eta_{sys3}$
[kW]	[%]	[%]	[%]
2	0.27	−0.62	−0.35
3	0.42	−0.51	−0.01
4	0.53	−0.48	0.06
5	0.61	−0.31	0.13
6	0.69	−0.15	0.27
7	0.91	0.18	0.63
8	2.65	1.61	1.61

Table 3. The gaps in fuel efficiency.

P_{load}	$\Delta Fuel_{eff1}$	$\Delta Fuel_{eff2}$	$\Delta Fuel_{eff3}$
[kW]	[W/lpm]	[W/lpm]	[W/lpm]
2	−1	−1.8	−15.3
3	−0.7	−1.5	−3
4	0.7	−0.7	−0.7
5	1.8	−0.5	0.4
6	2.5	−0.4	1.4
7	3.91	0.62	3.31
8	10.35	11.2	11.2

Table 4. Fuel economy.

P_{load}	$\Delta Fuel_{T1}$	$\Delta Fuel_{T2}$	$\Delta Fuel_{T3}$
[kW]	[L]	[L]	[L]
2	1.24	1.2	11.26
3	0.13	0.79	4.14
4	−0.13	0.77	2.08
5	−0.38	0.55	−0.08
6	−1.38	0.42	−2.28
7	−4.34	−0.14	−12.16
8	−11.8	−4	−28.48

The fuel economy are presented in Tables 5–7 for each strategy $RTOk$, $k = 1 \div 3$, compared to sFF strategy in case A ($k_{fuel} = 0$), B ($k_{fuel} = 25$), and C ($k_{fuel} = 50$) under constant load.

Table 5. Fuel economy for the RTO1 strategy using different k_{fuel} .

P_{load}	$\Delta Fuel_{T1A}$	$\Delta Fuel_{T1B}$	$\Delta Fuel_{T1C}$
[kW]	[L]	[L]	[L]
2	1.22	1.22	1.28
3	0.13	−0.25	0.1
4	−0.13	−0.71	−0.23
5	−0.38	−1.03	−0.48
6	−1.38	−2.08	−1.08
7	−4.34	−10.56	−3.56
8	−11.8	−22.92	−6.8

Table 6. Fuel economy for the RTO2 strategy using different k_{fuel} .

P_{load}	$\Delta Fuel_{T2A}$	$\Delta Fuel_{T2B}$	$\Delta Fuel_{T2C}$
[kW]	[L]	[L]	[L]
2	1.2	−0.09	1.22
3	0.79	−0.24	0.56
4	0.77	−0.25	0.42
5	0.55	−0.46	0.28
6	0.42	−1.58	0.22
7	−0.14	−4.24	−1.14
8	−4	−18.48	−8.48

Table 7. Fuel economy for the RTO3 strategy using different k_{fuel} .

P_{load}	$\Delta Fuel_{T3A}$	$\Delta Fuel_{T3B}$	$\Delta Fuel_{T3C}$
[kW]	[L]	[L]	[L]
2	11.26	12.14	7.628
3	4.14	5.548	2.764
4	2.08	1.2	0.288
5	−0.08	−6.44	−5.8
6	−2.28	−14.14	−13.02
7	−12.16	−28.42	−24.82
8	−28.48	−31.08	−29.8

For the RTO1, RTO2 and RTO3 strategies, the deficiencies of the FC electrical efficiency and for the fuel efficiency are shown in Figures 5 and 6. Fuel economy for the RTO1, RTO2, and RTO3 strategies in case A ($k_{fuel} = 0$), B ($k_{fuel} = 25$), and C ($k_{fuel} = 50$) under constant load is shown in Figures 7–9.

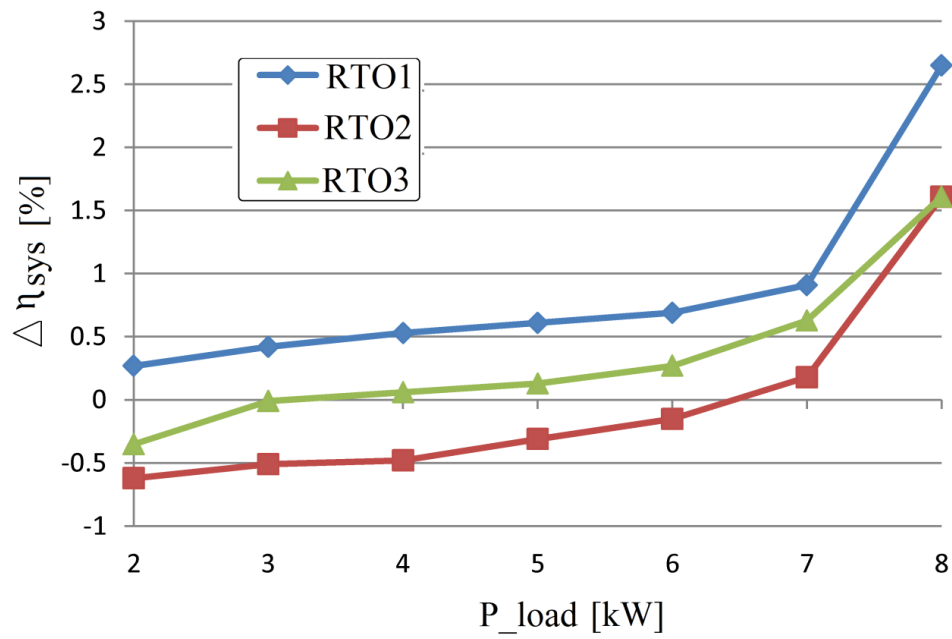


Figure 5. The gaps in FC electrical efficiency for the strategies RTO1, RTO2, and RTO3.

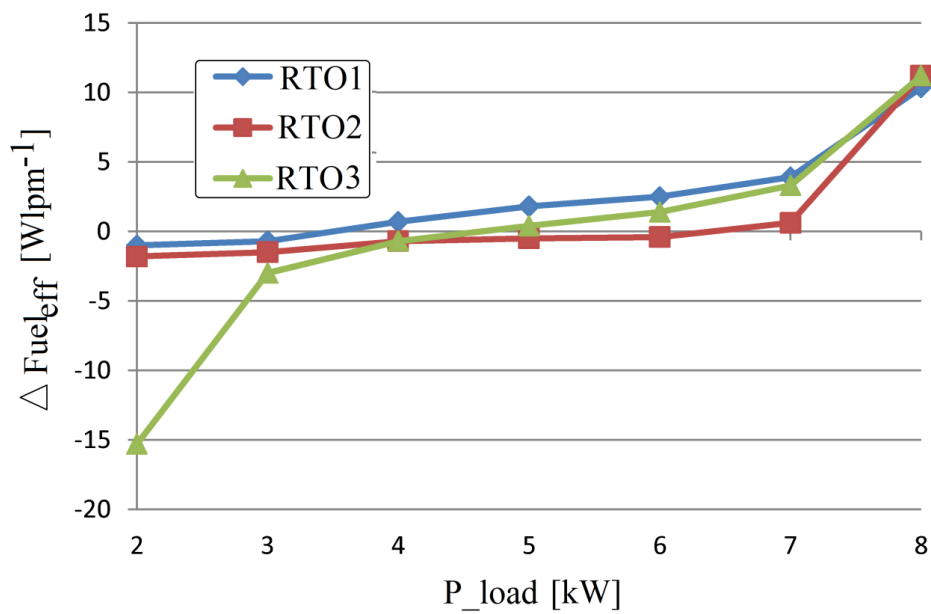


Figure 6. The deficiencies of the fuel efficiency for all RTO1, RTO2, and RTO3 strategies.

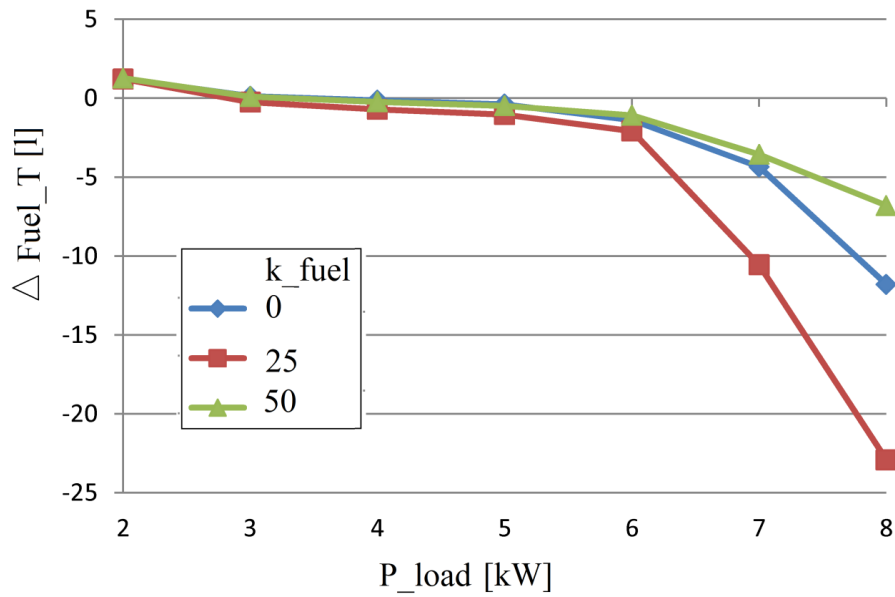


Figure 7. The values of the fuel economy, in the all situation, for the RTO1 strategy: A ($k_{\text{fuel}} = 0$), B ($k_{\text{fuel}} = 25$), and C ($k_{\text{fuel}} = 50$) under constant load.

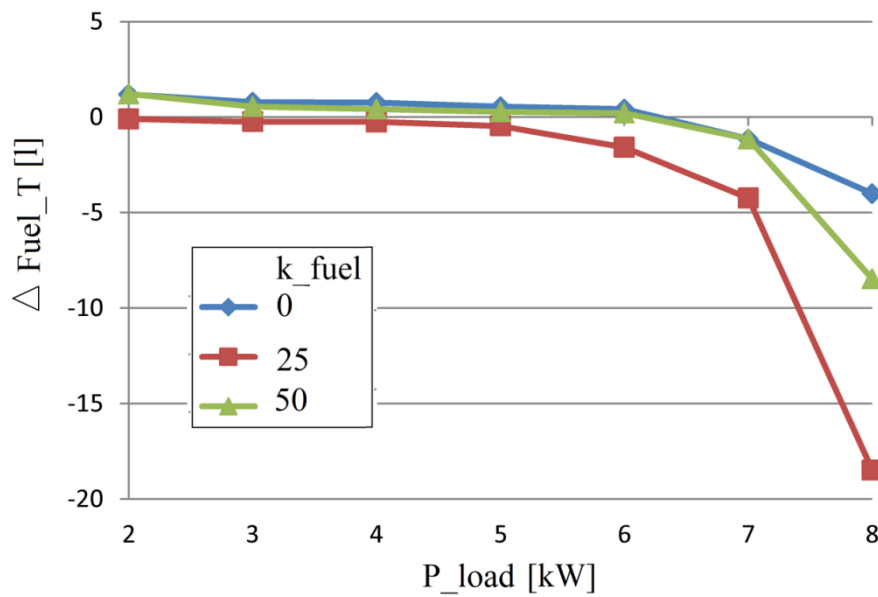


Figure 8. The values of the fuel economy, in the all situation, for the RTO2 strategy: A ($k_{\text{fuel}} = 0$), B ($k_{\text{fuel}} = 25$), and C ($k_{\text{fuel}} = 50$) under constant load.

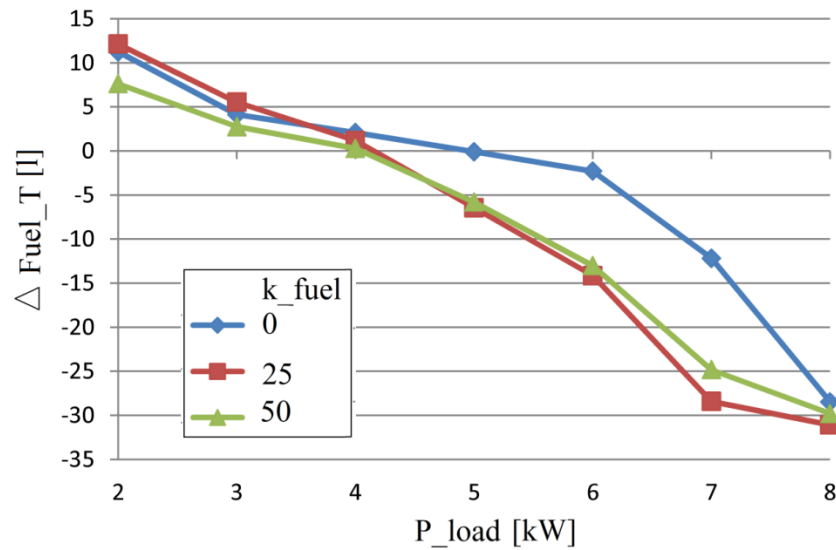


Figure 9. The values of the fuel economy, in the all situation, for the RTO3 strategy: A ($k_{fuel} = 0$), B ($k_{fuel} = 25$), and C ($k_{fuel} = 50$) under constant load.

The gaps in FC electric efficiency is positive in full range of the load demand for the RTO1 strategy and best compared to strategies RTO2 and RTO3 (see Figure 5). Also, the fuel efficiency for RTO1 strategy is better compared to strategies RTO2 and RTO3 (see Figure 6). Fuel economy for the strategies RTO1 and RTO2 has almost the same shapes of evolution with load demand. Almost the same values for light load, but different values for high load are obtained (see Figures 7 and 8). So, the FC net power could be maximized if the FC vehicle ascends up a hill using any of the RTO strategies outlined in this paper. Also, remember that the best fuel economy result for case B ($k_{fuel} = 25$), so the fuel economy could be maximized if the FC vehicle ascends up a hill by choosing the appropriate value for weighting parameter k_{fuel} . The performance of the RTO strategies outlined in this paper must be validated in different scenarios below.

4.2. Fuel Economy for the HPS under Variable Load Demand, $P_{RES} = 0$, and Different k_{fuel}

Only to exemplify that the LFW control of the boost converter operates based on (13), the behavior of the FC-HPS under 6.25 kW LC for the strategies RTO1 ($I_{ref(LFW)} = I_{ref(boost)}$, $I_{ref(Fuel)} = I_{refGES2} + I_{FC}$ and $I_{ref(Air)} = I_{FC}$) with $k_{fuel} = 25$ is presented in Figure 10.

The load cycles of 6.25 kW average power ($P_{load(AV)} = 6.25$ kW) is presented in first plot of Figure 10, but other load cycles that are used in this study as well, with different $P_{load(AV)}$ values mentioned in Table 8, are defined in [71]. The fuel economy $Fuel_{TO(LC)}$ for the sFF strategy is presented as reference in Table 8.

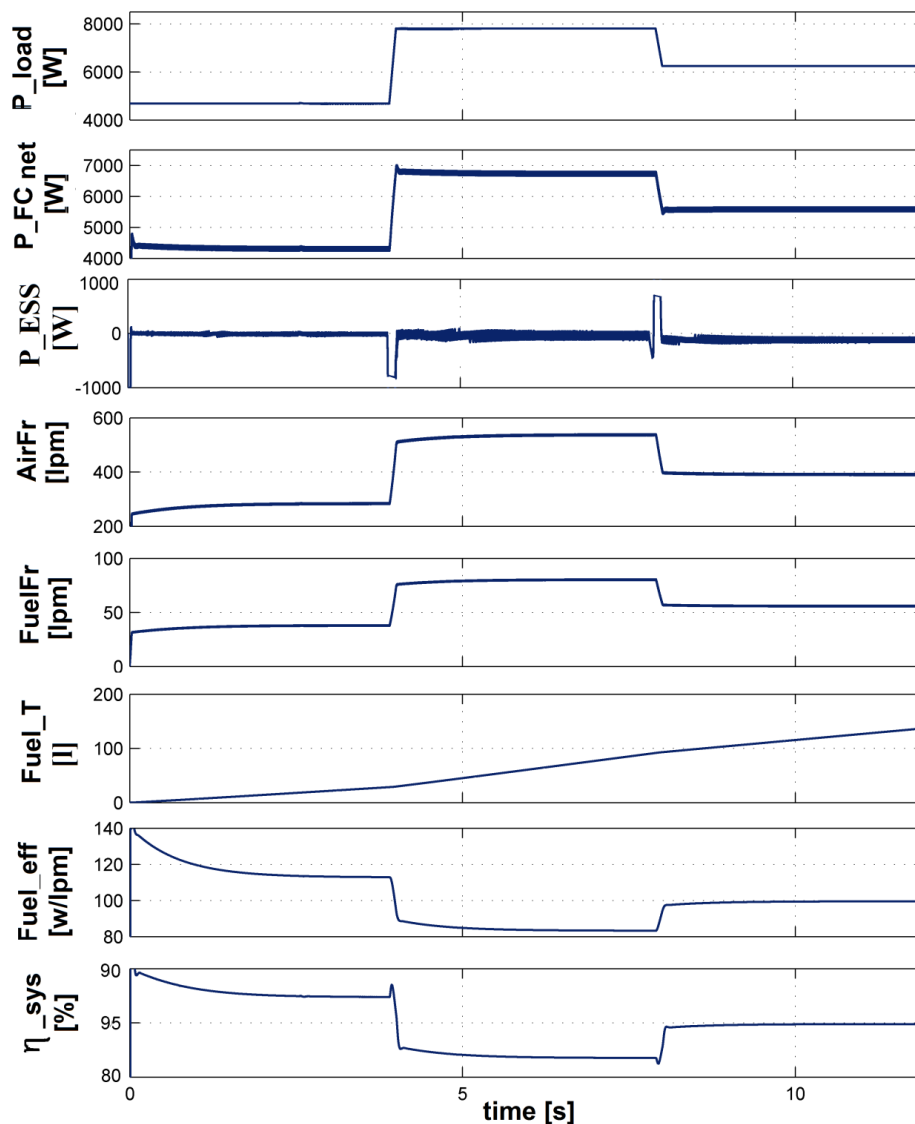


Figure 10. The behavior of the FC HPS under 6.25 kW LC (using RTO1 strategy with $k_{fuel} = 25$).

Table 8. The fuel economy $Fuel_{TO(LC)}$ for the sFF strategy.

LC Stage		$Fuel_{TO(LC)}$
$P_{load(AV)}$ [kW]		[L]
2		34.14
3		53.92
4		75.8
5		100.62
6		130.2
6.25		138.86

The structure of the Figure 10 is as follows: the first plot shows the variable profile of the load power (P_{Load}); the second plot shows the generated FC net power profile (P_{FCnet}) and this follows the load demand, highlighting that the LFW control operates properly; the third plot shows the ESS power, highlighting the advantage of LFW control implementing: the battery operating mode will only be of the charge-sustaining type ($P_{ESS(AV)} \cong 0$), the DC bus power flow balance being sustained only during sharp variation of the load demand; the next two plots show the fueling flow rates ($AirFr$ and $FuelFr$);

the last three plots show the fuel consumption ($Fuel_T$), the fuel efficiency ($\Delta Fuel_{eff}$), and the FC electric efficiency (η_{sys}). It is worth to mention that the shape of the signals for the strategies RTO1, RTO2, and RTO3 will look almost the same, but small differences in performance indicators can be observed for different LCs (which are mentioned in Table 9 for each RTO strategy). For example, the differences in FC net power ($\Delta P_{FCnet} = P_{FCnetk} - P_{FCnet0}$, $k = 1, 2, 3$), FC energy efficiency ($\Delta \eta_{sys} = \eta_{sysk} - \eta_{sys0}$), fuel efficiency ($\Delta Fuel_{eff} = Fuel_{effk} - Fuel_{eff0}$), and fuel economy ($\Delta Fuel_T = Fuel_{Tk} - Fuel_{T0}$) are represented in Figure 11 for RTO1 strategy with $k_{fuel} = 25$ (the value where the best fuel economy was obtained for constant load).

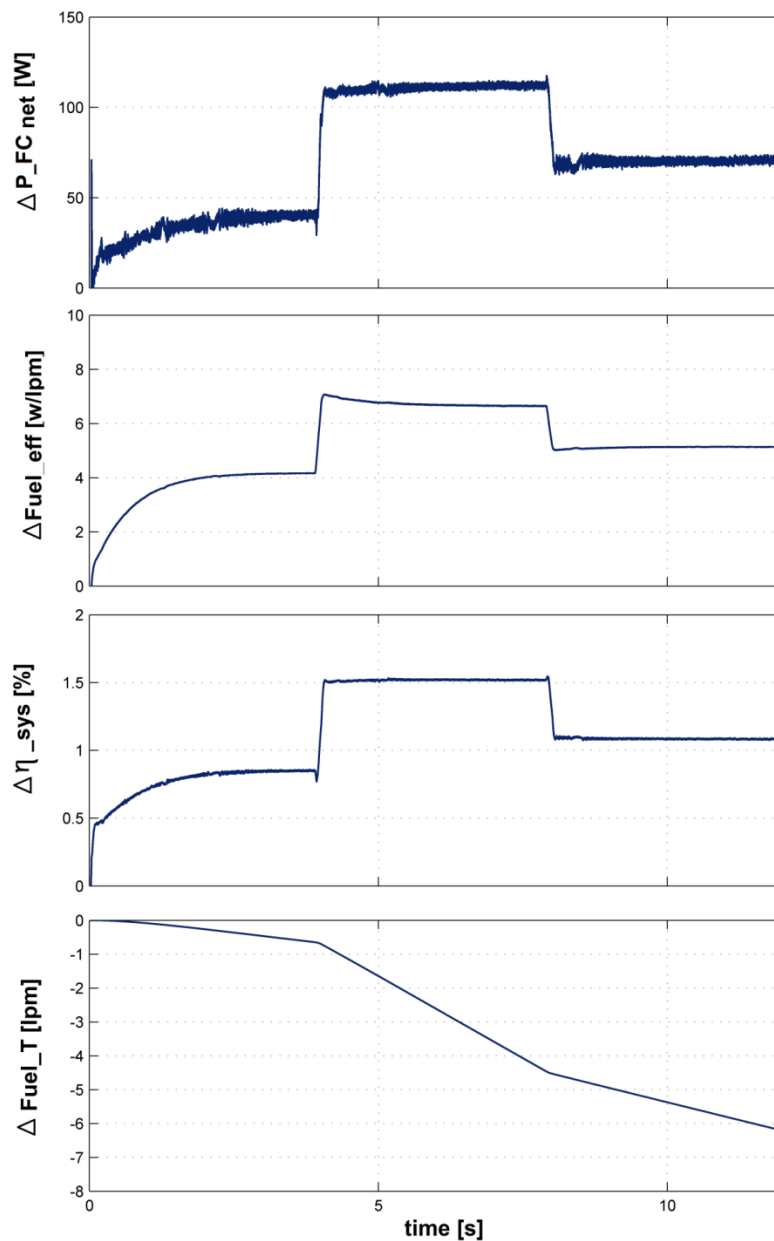


Figure 11. The behavior of the performance indicators for the FC HPS under 6.25 kW LC (using RTO1 strategy with $k_{fuel} = 25$).

The fuel economy for strategies RTO1 is of 6.36 liters (see also Table 10) and this performance indicator will be used to compare selected RTO strategies under variable load. The fuel economy is presented in Tables 9–11 for selected RTO strategies compared to sFF strategy.

Table 9. Fuel economy under variable load demand for the RTO1 strategy using different k_{fuel} .

$P_{load(AV)}$	$\Delta Fuel_{T(LC)1A}$	$\Delta Fuel_{T(LC)1B}$	$\Delta Fuel_{T(LC)1C}$
[kW]	[L]	[L]	[L]
2	1.3	0.5	0.51
3	0.71	−0.48	−0.47
4	0.07	−1.8	−1.58
5	−1.6	−3	−2.99
6	−3.8	−5.3	−5.23
6.25	−4.56	−6.36	−6.21

Table 10. Fuel economy under variable load demand for the RTO2 strategy using different k_{fuel} .

$P_{load(AV)}$	$\Delta Fuel_{T(LC)2A}$	$\Delta Fuel_{T(LC)2B}$	$\Delta Fuel_{T(LC)2C}$
[kW]	[L]	[L]	[L]
2	1.35	−0.51	−0.5
3	0.6	−0.75	−0.74
4	0.52	−1	−0.97
5	0.4	−1.2	−1.25
6	−0.2	−1.8	−1.72
6.25	−0.76	−2.06	−2.04

Table 11. Fuel economy under variable load demand for the RTO3 strategy using different k_{fuel} .

$P_{load(AV)}$	$\Delta Fuel_{T(LC)7A}$	$\Delta Fuel_{T(LC)7B}$	$\Delta Fuel_{T(LC)7C}$
[kW]	[L]	[L]	[L]
2	5.26	7.18	14.5
3	4.28	7.24	12.7
4	2.4	3.32	3.5
5	−4.38	−3.16	−2.34
6	−15.08	−13.28	−12.08
6.25	−19.1	−17.6	−16.32

The fuel economy for selected RTO strategy, in the all situation, A ($k_{net} = 0.5$, $k_{fuel} = 0$), B ($k_{net} = 0.5$, $k_{fuel} = 25$), and C ($k_{net} = 0.5$, $k_{fuel} = 50$), under variable load demand is shown in Figures 12–14.

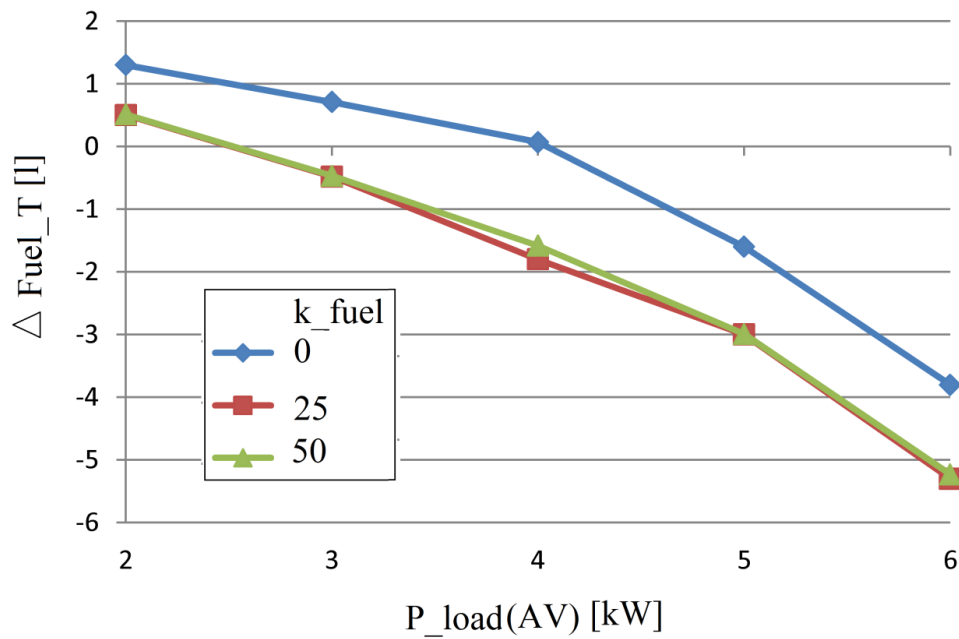


Figure 12. Fuel economy for the RTO1 strategy in case A ($k_{fuel} = 0$), B ($k_{fuel} = 25$), and C ($k_{fuel} = 25$) under variable load.

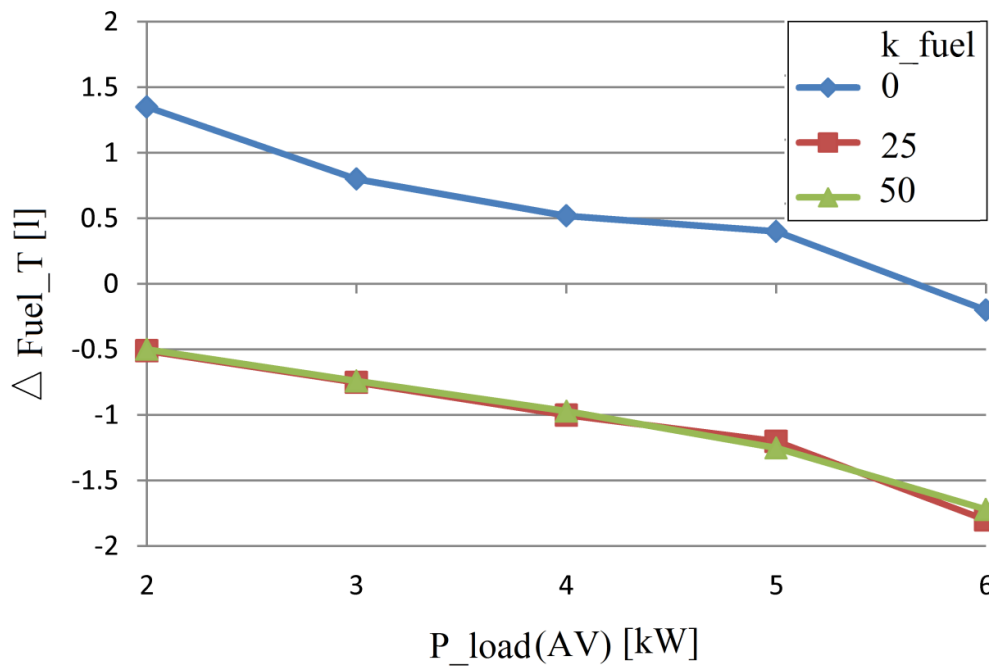


Figure 13. Fuel economy for the RTO2 strategy in case A ($k_{fuel} = 0$), B ($k_{fuel} = 25$), and C ($k_{fuel} = 25$) under variable load.

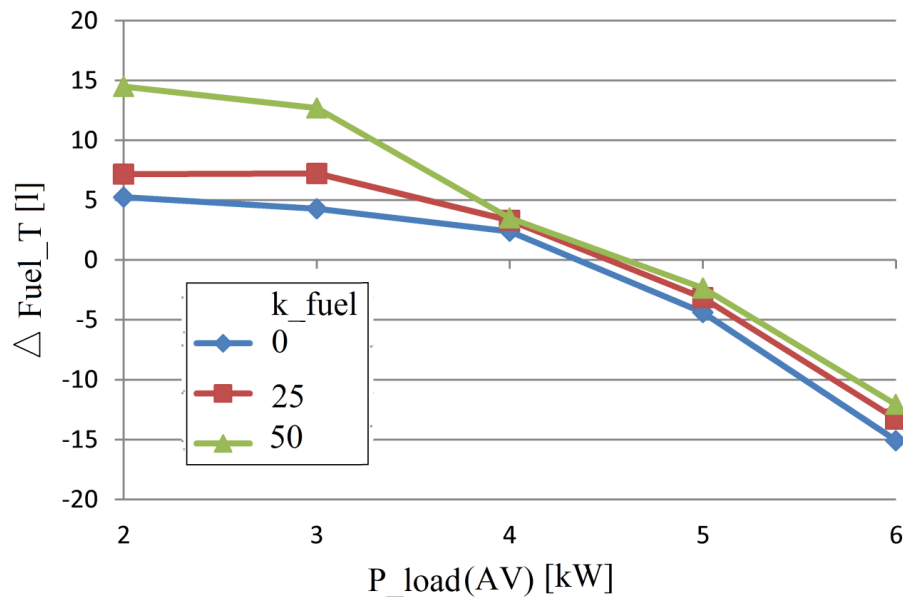


Figure 14. Fuel economy for the RTO3 strategy in case A ($k_{fuel} = 0$), B ($k_{fuel} = 25$), and C ($k_{fuel} = 25$) under variable load.

Note that the values for the fuel economy increases for some strategies, RTO1 and RTO2, only if $k_{fuel} \neq 0$. A sensitivity analysis was performed considering the parameter k_{fuel} with values between 10 and 50, for understand the shape of the optimization function in this variable k_{fuel} .

The results show that the optimization function is multimodal, with parameter k_{fuel} , so any value for k_{fuel} , between 10 and 50, can be used and the same fuel economy can be obtained for two different values of k_{fuel} . It is worth mentioning that any value of k_{fuel} in the range of values between 10 and 50 will improves the fuel economy for the strategies RTO1, in almost the full range of load demand and this is higher than that obtained with the RTO3 strategy, but no improvement in fuel economy at light load is obtained for RTO3 strategy if $k_{fuel} \neq 0$. Also, it worth to mention the the fuel economy is almost the same for $k_{fuel} = 0$ or $k_{fuel} \neq 0$ compared to sFF strategy for $P_{load(AV)} > 5$ kW (as it can be observed at constant load as well; see Figure 9), but clearly higher than that obtained with the booth strategies RTO1 respectively RTO2.

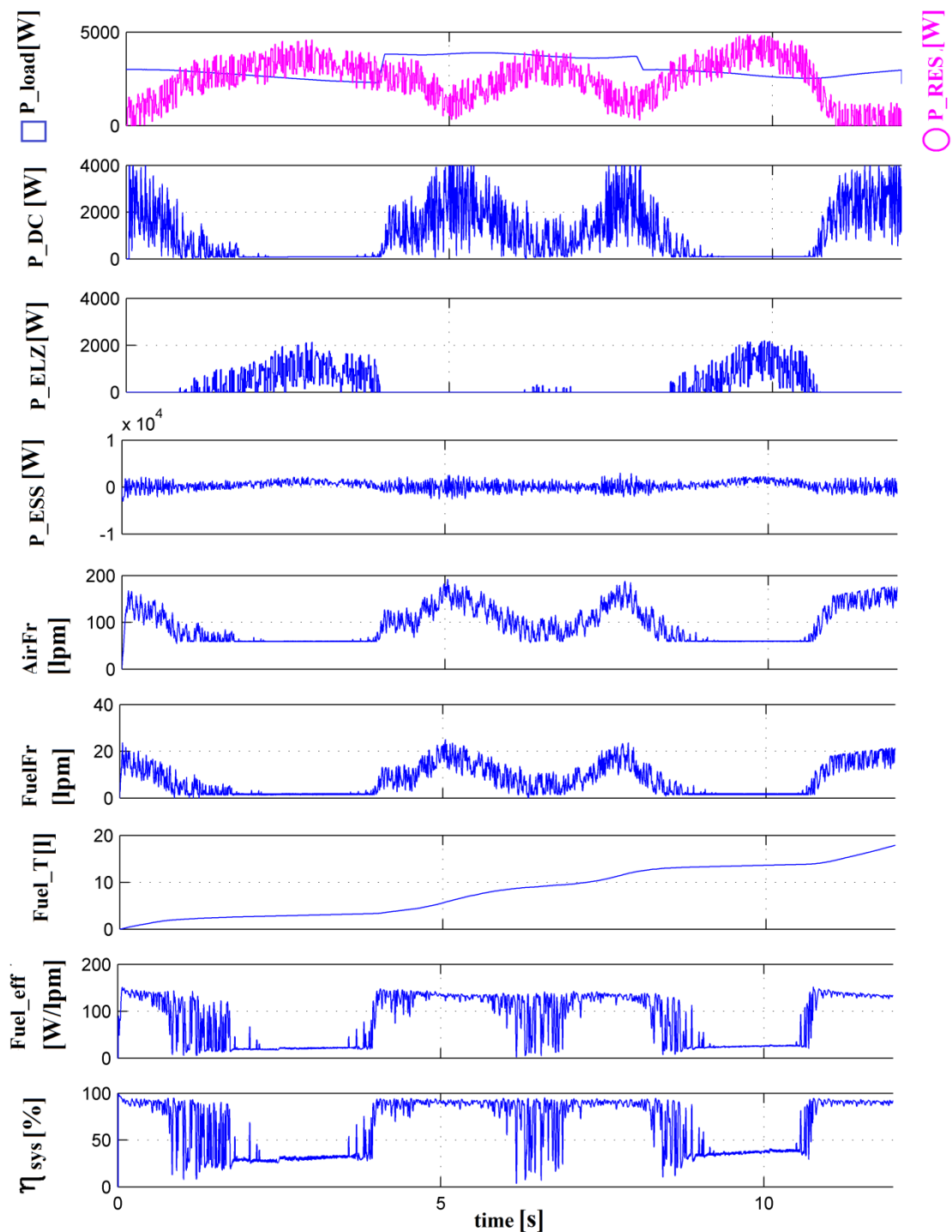
Consequently, the rules of the RTO switching strategy for best fuel economy of 6 kW FC-HPS could be defined as follows: (i) set the weighting coefficient k_{fuel} to optimum value (around of 25); (ii) if the load demand is lower than 5 kW then the recommended strategy must be the RTO1 strategy; (iii) if the load demand is higher than 5 kW then the recommended strategy must be the RTO3 strategy.

4.3. Fuel Economy for the HPS under Variable Load Demand and $P_{RES} \neq 0$

For exemplify, in Figure 15 is presented the functioning for the RTO3-based FC-HPS under variable load and RES power for two AV levels of the load demand ($P_{load(AV)} = 4$ kW and $P_{load(AV)} = 6$ kW in Figure 15a,b). The plots' organization presented in Figure 15 is: the first plot shows the profile of the load power. The second plot shows the FC net power profile. This FC net power follows the load demand due to the implemented LF control. The third plot shows the Energy Storage System power, highlighting the LF control advantage: the ESS operate in the charge sustaining manner ($P_{ESS(AV)} \cong 0$); the fueling flow rates ($AirFr$ and $FuelFr$) are presented in the next two plots, and, in the last three plots, the fuel consumption, the fuel efficiency, and the FC energy efficiency are presented.

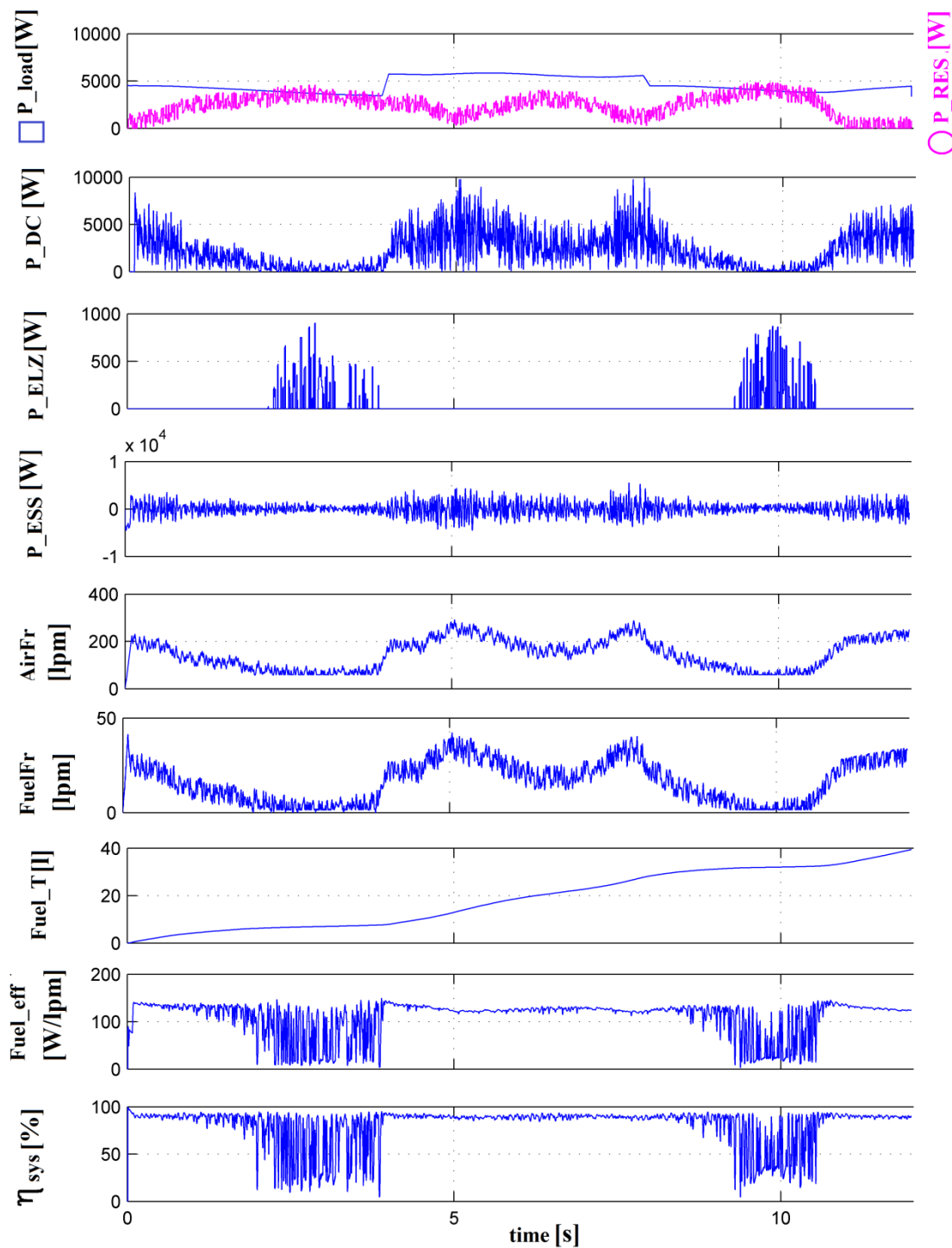
If the RES power is higher than the load demand ($P_{RES} > P_{load}$), the fuel cell operate in standby mode, at low power. This is done by limiting fueling flows, avoiding a more complicated star-stop procedure.

The resulting power excess, ($P_{RES} - P_{load}$) must be used (one use it to supply an electrolyzer). If this power excess is not used, it is necessary to monitor the charging state of the battery, in order to avoid full charging.



(a) $P_{load(AV)} = 4 \text{ kW}$ and $k_{fuel} = 25 \text{ W}^{-1} \text{ lpm}$

Figure 15. Cont.



(b) $P_{load(AV)} = 6 \text{ kW}$ and $k_{fuel} = 25 \text{ W}^{-1} \text{ lpm}$

Figure 15. The HPS behavior of the RTO3 strategy for P_{RES} variable, $k_{net} = 0.5 \text{ W}^{-1}$, $k_{fuel} = 25 \text{ W}^{-1} \text{ lpm}$, and different $P_{load(AV)}$.

5. Discussion

Differently from the sFF strategy, to explain the fuel economy obtained with the GTO-based RTO strategy, it is necessary follow the values of the performance indicators mentioned above and the values for the adjustment parameters and the gains. Taking into account design rules from [75], tuning parameters k_1 , respectively k_2 , were designed for fuel cell system with 6 kW power.

Normalization gains must to accommodate the booth values: y_N respectively p for the full range of searching. In this case, the following values were used in the simulation: $k_{Ny} = \frac{2}{Y_{Max}} \cong \frac{1}{3000}$ and $k_{Np} = \frac{I_{FC(rated)}}{2} \cong 60$. The following values for weighting coefficients $k_{net} = 0.5W^{-1}$ lmp, respectively $k_{fuel} = 25W^{-1}$ lpm were chosen to give an approximately identical contribution to FC net power ($k_{net} \cdot P_{FCnet} \cong 3000$), and for the fuel consumption efficiency ($k_{fuel} \cdot Fuel_{eff} \cong 25 \cdot 110 = 2750$) into the optimization function ($Y_{Max} = f \cong 5750$). The load demand varies in range of 2 kW to 8 kW and the FC current from 10 A to 240 A. Thus, considering these values, the optimization function varies from about 4400 to 6400. Thus, the signal y_N varies from 1.5 ($\cong \frac{4400}{3000}$) to 2.1 ($\cong \frac{6400}{3000}$) and the signal p from $\frac{1}{6}$ ($\frac{10}{60}$) to 4 ($\frac{240}{30}$). The adaptive characteristic of the GES control has 100% ability to discover the global optimum for these variations in the parameters [76,96].

Since the imposed objective is to improve the fuel cell net power, and not to save the fuel (the form of optimization function is $f = k_{net} \cdot P_{FCnet}$), we will get more fuel economy by using the sFF strategy, in comparison with RTO strategies if $k_{net} = 0$ and the load is lower ($P_{load} < 3kW$).

If the $P_{load} < 3$ kW, the results obtained are very little different when performing a sensitivity analysis in according with: $k_{fuel} \neq 0$. This is possible because we have low values for search resolution (RS), which become lower than 0.5% and hit count decreases (so a suboptimal value was found instead of the optimum).

Except for the RTO3's strategy at light load ($P_{load(AV)} < 4$ kW for $k_{fuel} \neq 0$), in all other cases, we achieve fuel economy, both for constant load and for variable load. The exception occurs when $R_S < 0.5\%$ at light load, but note, compared to strategies RTO1 and RTO2, the high fuel economy of RTO3 strategy that is obtained for $P_{load(AV)} > 4$ kW due to optimal control of the boost converter.

The multimodal characteristic of the optimization function in variable k_{fuel} resulted after the sensitivity analysis performed for different k_{fuel} values, in the 10–50 range. In this way, for any k_{fuel} value in the above mentioned range, the fuel economy can be improved.

Several factors influence tracking efficiency. These factors are: the dynamics of the load; the RES power profile; and last but not least, the tracking time (the response time of the search loop) [25–29].

As was mentioned, if we have a 100 Hz sinusoidal dither, 10 periods of dither (0.1 s) represent the tracking time for the GES control. Consequently, the dynamic phenomena such as the RES power fluctuation and high and sharp dynamics of load demand will influence the performance of any RTO strategy (including the sFF strategy) if the tracking time is not lower than time constants of the process under optimization. For the stationary tracking accuracy parameter, the following results are obtained: for stationary mode, and for the dither frequencies ranging from 10 Hz to 1000 Hz, we have an accuracy of 99.99%. If we have load pulses mode, and we have 100 Hz for the dither frequency, we obtain a tracking accuracy of 99.86%. This accuracy decreases to 98% if the dither frequency is 1000 Hz [78]. Taking into account the sensitivity analysis performed for the dither signal frequency in the interval between 10 Hz and 1000 Hz, the best results appear when we use a sinusoidal dither signal with a hundred Hz frequency.

For a fair comparison, the LFW reference $I_{ref(LFW)}$ was used as reference input for the boost controller ($I_{ref(boost)}$) in the strategies RTO1 and RTO2, and for air regulator in RTO3 strategy. The inputs of the air regulator ($I_{ref(Air)}$) and the fuel regulator ($I_{ref(Fuel)}$) in the strategies RTO1 and RTO2 were controlled by the GES reference ($I_{ref(GES)}$) and the FC current (I_{FC}) to optimize the FC system operation as follows: the RTO1 strategy uses $I_{ref(Fuel)} = I_{ref(GES)} + I_{FC}$ and $I_{ref(Air)} = I_{FC}$, and the RTO2 strategy uses $I_{ref(Air)} = I_{ref(GES)} + I_{FC}$ and $I_{ref(Fuel)} = I_{FC}$. The RTO3 strategy uses $I_{ref(boost)} = I_{ref(GES)}$, $I_{ref(Air)} = I_{ref(LFW)}$, and $I_{ref(Fuel)} = I_{FC}$. Thus, the RTO3 strategy uses the boost converter to optimize the FC system operation, which has response time much shorter than the fueling regulators and speed advantage in searching the optimum of the optimization function compared to strategies RTO1 and RTO2. Consequently, for best fuel economy, the potential rules of an advanced RTO switching can be defined as follows: (i) set the weighting coefficient $k_{fuel} \neq 0$ (in range 10 to 50); (ii) if the load demand

is lower than 5 kW then the recommended strategy must be the RTO1 strategy; (iii) if the load demand is higher than 5 kW then the recommended strategy must be the RTO3 strategy.

The next work will be focused on a comparative analysis of the fuel economy obtained by using the RTO strategies proposed in this paper with those analyzed in [71].

6. Conclusions

In this paper, besides a brief presentation of current RTO strategies and a critical assessment of proposed Extremum Seeking (ES) algorithms, the fuel economy of three Renewable Fuel Cell Hybrid Power System (REW/FC-HPS) topologies has been analyzed.

In this paper, the dynamics on load demand and the electric power available from the Renewable Energy Sources (RESs), is proposed to be mitigated using the load-following (LFW) control in order to sustain the power flow balance on the DC bus within much power support from the battery. Because, in this case, the battery will work in charge-sustained mode, resulting clear advantages for FC vehicles related to battery size, its lifetime and maintenance cost.

The optimization objective can be set in real-time by changing the values of the weighting coefficients k_{net} and k_{fuel} in order to increase the overall fuel economy, the FC electrical efficiency, or other performance indicators defined for the HPS.

So, besides the proposal of the switching RTO strategy, the main results of this study can be summed up as follows:

- In comparison with sFF strategy, the control strategies RTO1 and RTO2 offers a higher FC electric efficiency for all range of the load demand (see Figure 5).
- The fuel efficiency of the strategies RTO1 and RTO3 is almost the same for $P_{load(AV)} > 4$ kW (see Figure 6).
- The fuel economy of all RTO strategies analyzed here for $k_{fuel} = 0$ is almost the same for $P_{load(AV)} < 4$ kW, but a three times higher fuel economy is achieved at maximum load considering the RTO3 strategy compared to RTO1 strategy (see Figures 7–9 for $k_{fuel} = 0$).
- The fuel economy increases even further if $k_{fuel} \neq 0$ (see Figures 7–9).
- The conclusions about fuel economy for each RTO strategy remain the same for variable profiles of the load demand and RES power.
- The variability of the RES power and load dynamics can be mitigated by the LFW proposed in this paper to sustain the power flow balance on the DC bus without much support from the batteries' stack, which mainly operates in charge-sustained mode.

Finally, it worth to mention that exploration of space of the optimal solutions with two variables could have as result a higher fuel economy compared with one variable—based RTO strategies analyzed in this paper, but this assumption must further investigated.

Author Contributions: Conceptualization, Methodology, Validation, and Writing—Original Draft Preparation: B.N.; Writing—Review & Editing: O.M. and B.N.

Funding: This work was founded by two grants of the Ministry of National Education and Scientific Research, CNCS/CCCDI-UEFISCDI, within PNCDI III, code PN-III P1-1.2-PCCDI2017-0332 and title “Increasing the institutional capacity of bioeconomic research for the innovative exploitation of the indigenous vegetal resources in order to obtain horticultural products with high added value”, and within RDI Program for Space Technology and Advanced Research - STAR, code 167/2017 and title “Concept Development of an Energy Storage Unit Using High Temperature Superconducting Coil for Spacecraft Power Systems (SMESinSpace). The sponsors had no role in the design, execution, interpretation, or writing of the study. The research was performed in Research Center “Modeling and Simulation of the Systems and Processes”.

Conflicts of Interest: The authors declare no conflict of interest.

Nomenclature

$AirFr$	Air Flow rate
AV	Average value
BPF	Band-Pass Filter
f_d	Dither frequency
DP	Dynamic Programming
ECMS	Equivalent Consumption Minimization Strategy
EMS	Energy Management Strategy
EMU	Energy Management Unit
ES	Extremum Seeking
aPESC	Asymptotic Perturbed Extremum Seeking Control
PESCs	Scalar PESC
ESS	Energy Storage System
$FuelFr$	Fuel Flow rate
FC	Fuel cell
P_{FC}	FC stack power
P_{FCnet}	FC net power
P_{cm}	Air compressor power
$\eta_{\sigma\psi\sigma}$	FC electrical efficiency
eff_{H_2}	Hydrogen consumption efficiency
FC HPS	Fuel Cell Hybrid Power Systems
$FuelFr$	Fuel Flow rate
$Fuel_T$	Total Fuel Consumption
$Fuel_{eff}$	Fuel Consumption Efficiency
FFT	Fast Fourier Transform
FES	Flywheel energy storage
GES	Global Extremum Seeking
GaPESC	Global aPESC
HILS	Hardware-in-Loop System
HPF	High-Pass Filter
HPS	Hybrid Power System
k_{Np}	Output normalization gain
k_{Ny}	Input normalization gain
LC	Load Cycle
LFW	Load-Following
MEP	Maximum Efficiency Point
MPP	Maximum Power Point
MV	Mean Value
MPC	Model Predictive Control
MRAC	Model Reference Adaptive Control
PESC	Perturbed Extremum Seeking Control
PMP	Pontryagin's Minimum Principle
PEMFC	Proton Exchange Membrane Fuel
P_{Load}	Stationary load power (constant power demand)
p_{Load}	Dynamic load power (variable power demand)
RTO	Real-Time Optimization
RES	Renewable Energies Source
S_R	Searching Resolution
sFF	Static Feed-Forward
SMES	Superconducting Magnetic Energy Storage
SOC	State-Of-Charge
T_{acc}	Tracking accuracy
WT	Wind Turbines

References

1. Bizon, N.; Tabatabaei, N.M.; Blaabjerg, F.; Kurt, E. *Energy Harvesting and Energy Efficiency: Technology, Methods and Applications*; Springer: London, UK, 2017; Available online: <http://www.springer.com/us/book/9783319498744> (accessed on 12 December 2018).
2. Ijaodola, O.; Ogungbemi, E.; Khatib, F.N.; Wilberforce, T.; Ramadan, M.; Hassan, Z.E.; Thompson, J.; Olabi, A.G. Evaluating the Effect of Metal Bipolar Plate Coating on the Performance of Proton Exchange Membrane Fuel Cells. *Energies* **2018**, *11*, 3203. [[CrossRef](#)]
3. Rafique, M.K.; Haider, Z.M.; Mehmood, K.K.; Zaman, M.S.U.; Irfan, M.; Khan, S.U.; Kim, C.-H. Optimal Scheduling of Hybrid Energy Resources for a Smart Home. *Energies* **2018**, *11*, 3201. [[CrossRef](#)]
4. Sikkabut, S.; Mungporn, P.; Ekkaravardome, C.; Bizon, N.; Tricoli, P.; Nahid-Mobarakkeh, B.; Pierfederici, S.; Davat, B.; Thounthong, P. Control of High-Energy High-Power Densities Storage Devices by Li-ion Battery and Supercapacitor for Fuel Cell/Photovoltaic Hybrid Power Plant for Autonomous System Applications. *IEEE Trans. Ind. Appl.* **2017**, *52*, 4395–4407. [[CrossRef](#)]
5. Ishaque, K.; Salam, Z. A review of maximum power point tracking techniques of PV system for uniform insolation and partial shading condition. *Renew. Sustain. Energy Rev.* **2013**, *19*, 475–488. [[CrossRef](#)]
6. Liu, Z.-H.; Chen, J.-H.; Huang, J.-W. A review of maximum power point tracking techniques for use in partially shaded conditions. *Renew. Sustain. Energy Rev.* **2015**, *41*, 436–453. [[CrossRef](#)]
7. Bizon, N.; Tabatabaei, N.M.; Shayeghi, H. *Analysis, Control and Optimal Operations in Hybrid Power Systems—Advanced Techniques and Applications for Linear and Nonlinear Systems*; Springer: London, UK, 2013.
8. Olatomiwa, L.; Mekhilef, S.; Ismail, M.S.; Moghavvemi, M. Energy management strategies in hybrid renewable energy systems: A review. *Renew. Sustain. Energy Rev.* **2016**, *62*, 821–835. [[CrossRef](#)]
9. Zhang, P.; Yan, F.; Du, C. A comprehensive analysis of energy management strategies for hybrid electric vehicles based on bibliometrics. *Renew. Sustain. Energy Rev.* **2015**, *48*, 88–104. [[CrossRef](#)]
10. Peng, J.; He, H.; Xiong, R. Rule based energy management strategy for a series-parallel plug-in hybrid electric bus optimized by dynamic programming. *Appl. Energy* **2017**, *185*, 1633–1643. [[CrossRef](#)]
11. Das, V.; Padmanaban, S.; Venkitesamy, K.; Selvamuthukumar, R.; Siano, P. Recent advances and challenges of fuel cell based power system architectures and control—A review. *Renew. Sustain. Energy Rev.* **2017**, *73*, 10–18. [[CrossRef](#)]
12. Bizon, N.; Kurt, E. Performance Analysis of the Tracking of Global Extreme on Multimodal Patterns using the Asymptotic Perturbed Extremum Seeking Control Scheme. *Int. J. Hydrogen Energy* **2017**, *42*, 17645–17654. [[CrossRef](#)]
13. Ettihir, K.; Boulon, L.; Agbossou, K. Optimization-based energy management strategy for a fuel cell/battery hybrid power system. *Appl. Energy* **2016**, *163*, 142–153. [[CrossRef](#)]
14. Ettihir, K.; Cano, M.H.; Boulon, L.; Agbossou, K. Design of an adaptive EMS for fuel cell vehicles. *Int. J. Hydrogen Energy* **2017**, *42*, 1481–1489. [[CrossRef](#)]
15. Zhang, W.; Li, J.; Xu, L.; Ouyang, M. Optimization for a fuel cell/battery/capacity tram with equivalent consumption minimization strategy. *Energy Convers. Manag.* **2017**, *134*, 59–69. [[CrossRef](#)]
16. Raga, C.; Barrado, A.; Miniguano, H.; Lazaro, A.; Quesada, I.; Martin-Lozano, A. Analysis and Sizing of Power Distribution Architectures Applied to Fuel Cell Based Vehicles. *Energies* **2018**, *11*, 2597. [[CrossRef](#)]
17. Wiczorek, M.; Lewandow, M. A mathematical representation of an energy management strategy for hybrid energy storage system in electric vehicle and real time optimization using a genetic algorithm. *Appl. Energy* **2017**, *192*, 222–233. [[CrossRef](#)]
18. Harrag, A.; Bahri, H. Novel neural network IC-based variable step size fuel cell MPPT controller: Performance, efficiency and lifetime improvement. *Int. J. Hydrogen Energy* **2017**. [[CrossRef](#)]
19. Thounthong, P.; Luksanasakul, A.; Koseeyaporn, P.; Davat, B. Intelligent Model-Based Control of a Standalone Photovoltaic/Fuel Cell Power Plant with Supercapacitor Energy Storage. *IEEE Trans. Sustain. Energy* **2013**, *4*, 240–249. [[CrossRef](#)]
20. Huang, Y.; Wang, H.; Khajepour, A.; He, H.; Ji, J. Model predictive control power management strategies for HEVs: A review. *J. Power Sources* **2017**, *341*, 91–106. [[CrossRef](#)]
21. Wang, H.; Huang, Y.; Khajepour, A.; Song, Q. Model predictive control-based energy management strategy for a series hybrid electric tracked vehicle. *Appl. Energy* **2016**, *182*, 105–114. [[CrossRef](#)]

22. Matraji, I.; Ahmed, F.S.; Laghrouche, S.; Wack, M. Comparison of robust and adaptive second order sliding mode control in PEMFC air-feed systems. *Int. J. Hydrogen Energy* **2015**, *40*, 9491–9504. [[CrossRef](#)]
23. Mungporn, P.; Poonnoi, N.; Sikkabut, S.; Ekkaravarodome, E.; Thounthong, P.; Bizon, N.; Hinaje, M.; Pierfederici, S.; Davat, B. Model Based Control of Modified Four-Phase Interleaved Boost Converter for Fuel Cell Power Source for Mobile Based Station. In Proceedings of the International Telecommunications Energy Conference (INTELEC), Osaka, Japan, 18–22 October 2015.
24. Han, J.; Park, Y.; Dongsuk, K. Optimal adaptation of equivalent factor of equivalent consumption minimization strategy for fuel cell hybrid electric vehicles under active state inequality constraints. *J. Power Sources* **2014**, *267*, 491–502. [[CrossRef](#)]
25. Bassam, A.M.; Phillips, A.B.; Turnock, S.R.; Wilson, P.A. Development of a multi-scheme energy management strategy for a hybrid fuel cell driven passenger ship. *Int. J. Hydrogen Energy* **2017**, *42*, 623–635. [[CrossRef](#)]
26. Tribioli, L.; Cozzolino, R.; Barbieri, M. Optimal control of a repowered vehicle: Plug-in fuel cell against plug-in hybrid electric powertrain. *AIP Conf. Proc.* **2015**, *1648*, 570014. [[CrossRef](#)]
27. Hou, C.; Ouyang, M.G.; Xu, L.F.; Wang, H.W. Approximate Pontryagin’s minimum principle applied to the energy management of plug-in hybrid electric vehicles. *Appl. Energy* **2014**, *115*, 174–189. [[CrossRef](#)]
28. Ariyur, K.B.; Krstic, M. *Real-Time Optimization by Extremum-Seeking Control*; Wiley-Interscience: Hoboken, NJ, USA, 2003.
29. Ramos-Paja, C.A.; Spagnuolo, G.; Petrone, G.; Emilio Mamarelis, M. A perturbation strategy for fuel consumption minimization in polymer electrolyte membrane fuel cells: Analysis, Design and FPGA implementation. *Appl. Energy* **2014**, *119*, 21–32. [[CrossRef](#)]
30. Bizon, N. Energy harvesting from the FC stack that operates using the MPP tracking based on modified extremum seeking control. *Appl. Energy* **2013**, *104*, 326–336. [[CrossRef](#)]
31. Bizon, N. Improving the PEMFC energy efficiency by optimizing the fueling rates based on extremum seeking algorithm. *Int. J. Hydrogen Energy* **2014**, *39*, 10641–10654. [[CrossRef](#)]
32. Bizon, N. Tracking the maximum efficiency point for the FC system based on extremum seeking scheme to control the air flow. *Appl. Energy* **2014**, *129*, 147–157. [[CrossRef](#)]
33. Zhou, D.; Ravey, A.; Al-Durra, A.; Gao, F. A comparative study of extremum seeking methods applied to online energy management strategy of fuel cell hybrid electric vehicles. *Energy Convers. Manag.* **2017**, *151*, 778–790. [[CrossRef](#)]
34. Bizon, N. Global Maximum Power Point Tracking (GMPPT) of Photovoltaic array using the Extremum Seeking Control (ESC): A review and a new GMPPT ESC scheme. *Renew. Sustain. Energy Rev.* **2016**, *57*, 524–539. [[CrossRef](#)]
35. Bizon, N. Global Extremum Seeking Control of the Power Generated by a Photovoltaic Array under Partially Shaded Conditions. *Energy Convers. Manag.* **2016**, *109*, 71–85. [[CrossRef](#)]
36. Bizon, N. Global Maximum Power Point Tracking based on new Extremum Seeking Control scheme. *Prog. Photovolt. Res. Appl.* **2016**, *24*, 600–622. [[CrossRef](#)]
37. Bizon, N. Searching of the Extreme Points on Photovoltaic Patterns using a new Asymptotic Perturbed Extremum Seeking Control scheme. *Energy Convers. Manag.* **2017**, *144*, 286–302. [[CrossRef](#)]
38. Bizon, N. Load-following Mode Control of a Standalone Renewable/Fuel Cell Hybrid Power Source. *Energy Convers. Manag.* **2014**, *77*, 763–772. [[CrossRef](#)]
39. Tribioli, L.; Cozzolino, R.; Evangelisti, L.; Bella, G. Energy Management of an Off-Grid Hybrid Power Plant with Multiple Energy Storage Systems. *Energies* **2016**, *9*, 661. [[CrossRef](#)]
40. Cano, M.H.; Mousli, M.I.A.; Kelouwani, K.; Agbossou, K.; Dubé, Y. Improving a free air breathing proton exchange membrane fuel cell through the Maximum Efficiency Point Tracking method. *J. Power Sources* **2017**, *345*, 264–274. [[CrossRef](#)]
41. Ahmadi, S.; Abdi, S.; Kakavand, M. Maximum power point tracking of a proton exchange membrane fuel cell system using PSO-PID controller. *Int. J. Hydrogen Energy* **2017**, *42*, 20430–20443. [[CrossRef](#)]
42. Hernández-Torres, D.; Riu, D.; Sename, O. Reduced-order Robust Control of a Fuel Cell Air Supply System. *IFAC-PapersOnLine* **2017**, *50*, 96–101. [[CrossRef](#)]
43. Daud, W.R.W.; Rosli, R.E.; Majlan, E.H.; Hamid, S.A.A.; Mohamed, R.; Husaini, T. PEM fuel cell system control: A review. *Renew. Energy* **2017**, *113*, 620–638. [[CrossRef](#)]
44. Fathabadi, H. Novel fast and high accuracy maximum power point tracking method for hybrid photovoltaic/fuel cell energy conversion systems. *Renew. Energy* **2017**, *106*, 232–242. [[CrossRef](#)]

45. Eriksson, E.L.V.; Gray, E.M. Optimization and integration of hybrid renewable energy hydrogen fuel cell energy systems—A critical review. *Appl. Energy* **2017**, *202*, 348–364. [[CrossRef](#)]
46. Vivas, F.J.; De las Heras, A.; Segura, F.; Andújar, J.M. A review of energy management strategies for renewable hybrid energy systems with hydrogen backup. *Renew. Sustain. Energy Rev.* **2017**, *82*, 126–155. [[CrossRef](#)]
47. Tiar, M.; Betka, A.; Drid, S.; Abdeddaim, S.; Tabandjat, A. Optimal energy control of a PV-fuel cell hybrid system. *Int. J. Hydrogen Energy* **2017**, *42*, 1456–1465. [[CrossRef](#)]
48. Muñoz, P.M.; Correa, G.; Gaudiano, M.E.; Fernández, D. Energy management control design for fuel cell hybrid electric vehicles using neural networks. *Int. J. Hydrogen Energy* **2017**. [[CrossRef](#)]
49. Fernández, R.Á.; Caraballo, S.C.; Cilleruelo, F.B.; Lozano, J.A. Fuel optimization strategy for hydrogen fuel cell range extender vehicles applying genetic algorithms. *Renew. Sustain. Energy Rev.* **2018**, *81*, 655–668. [[CrossRef](#)]
50. Zhou, D.; Al-Durra, A.; Gao, F.; Ravey, A.; Matraji, I.; Simões, M.G. Online energy management strategy of fuel cell hybrid electric vehicles based on data fusion approach. *J. Power Sources* **2017**, *366*, 278–291. [[CrossRef](#)]
51. Caux, S.; Gaoua, Y.; Lopez, P. A combinatorial optimisation approach to energy management strategy for a hybrid fuel cell vehicle. *Energy* **2017**, *133*, 219–230. [[CrossRef](#)]
52. Han, J.; Yu, S.; Yi, S. Adaptive control for robust air flow management in an automotive fuel cell system. *Appl. Energy* **2017**, *190*, 73–83. [[CrossRef](#)]
53. Koubaa, R.; krichen, L. Double layer metaheuristic based energy management strategy for a Fuel Cell/Ultra-Capacitor hybrid electric vehicle. *Energy* **2017**, *133*, 1079–1093. [[CrossRef](#)]
54. Carignano, M.; Costa-Castelló, R.; Nigro, N.; Junco, S. A Novel Energy Management Strategy for Fuel-Cell/Supercapacitor Hybrid Vehicles. *IFAC-PapersOnLine* **2017**, *50*, 10052–10057. [[CrossRef](#)]
55. Bizon, N. FC energy harvesting using the MPP tracking based on advanced extremum seeking control. *Int. J. Hydrogen Energy* **2013**, *38*, 1952–1966. [[CrossRef](#)]
56. Pukrushpan, J.T.; Stefanopoulou, A.G.; Peng, H. *Control of Fuel Cell Power Systems*; Springer: London, UK, 2004.
57. Matraji, I.; Laghrouche, S.; Jemei, S.; Wack, M. Robust control of the PEM fuel cell air-feed system via sub-optimal second order sliding mode. *Appl. Energy* **2013**, *104*, 945–957. [[CrossRef](#)]
58. Laghrouche, S.; Matraji, I.; Ahmed, F.S.; Jemei, S.; Wack, M. Load governor based on constrained extremum seeking for PEM fuel cell oxygen starvation and compressor surge protection. *Int. J. Hydrogen Energy* **2013**, *38*, 14314–14322. [[CrossRef](#)]
59. Kunusch, C.; Puleston, P.F.; Mayosky, M.A.; Fridman, L. Experimental results applying second order sliding mode control to a PEM fuel cell based system. *Control Eng. Pract.* **2013**, *21*, 719–726. [[CrossRef](#)]
60. Zhao, D.; Zheng, Q.; Gao, F.; Bouquain, D.; Dou, M.; Miraoui, A. Disturbance decoupling control of an ultra-high speed centrifugal compressor for the air management of fuel cell systems. *Int. J. Hydrogen Energy* **2014**, *39*, 1788–1798. [[CrossRef](#)]
61. Da Fonseca, R.; Bideaux, E.; Gerard, M.; Jeanneret, B.; Desbois-Renaudin, M.; Sari, A. Control of PEMFC system air group using differential flatness approach: Validation by a dynamic fuel cell system model. *Appl. Energy* **2014**, *113*, 219–229. [[CrossRef](#)]
62. Zhou, N.; Yang, C.; Tucker, D.; Pezzini, P.; Traverso, A. Transfer function development for control of cathode airflow transients in fuel cell gas turbine hybrid systems. *Int. J. Hydrogen Energy* **2015**, *40*, 1967–1979. [[CrossRef](#)]
63. Nikezhadi, A.; Fantova, M.A.; Kunusch, C.; Martinez, C.O. Design and implementation of LQR/LQG strategies for oxygen stoichiometry control in PEM fuel cells based systems. *J. Power Sources* **2011**, *196*, 4277–4282. [[CrossRef](#)]
64. Ou, K.; Wang, Y.X.; Li, Z.Z.; Shen, Y.D. Feedforward fuzzy-PID control for air flow regulation of PEM fuel cell system. *Int. J. Hydrogen Energy* **2015**, *40*, 11686–11695. [[CrossRef](#)]
65. Beirami, H.; Shabestari, A.Z.; Zerafat, M.M. Optimal PID plus fuzzy controller design for a PEM fuel cell air feed system using the self-adaptive differential evolution algorithm. *Int. J. Hydrogen Energy* **2015**, *40*, 9422–9434. [[CrossRef](#)]
66. Wang, Y.Z.; Xuan, D.J.; Kim, Y.B. Design and experimental implementation of time delay control for air supply in a polymer electrolyte membrane fuel cell system. *Int. J. Hydrogen Energy* **2013**, *38*, 13381–13392. [[CrossRef](#)]

67. Bizon, N. Energy Efficiency of Multiport Power Converters used in Plug-In/V2G Fuel Cell Vehicles. *Appl. Energy* **2012**, *96*, 431–443. [[CrossRef](#)]
68. Won, J.S.; Langari, R. Intelligent energy management agent for a parallel hybrid vehicle-part II: Torque distribution, charge sustenance strategies, and performance results. *IEEE Trans. Veh. Technol.* **2005**, *54*, 935–953. [[CrossRef](#)]
69. Pisu, P.; Rizzoni, G. A comparative study of supervisory control strategies for hybrid electric vehicles. *IEEE Trans. Control Syst. Technol.* **2007**, *15*, 506–518. [[CrossRef](#)]
70. Musardo, C.; Rizzoni, G.; Guezennec, Y.; Staccia, B. A-ECMS: An Adaptive Algorithm for Hybrid Electric Vehicle Energy Management. *Eur. J. Control* **2005**, *11*, 509–524. [[CrossRef](#)]
71. Bizon, N.; Lopez-Guede, J.M.; Kurt, E.; Thounthong, P.; Mazare, A.G.; Ionescu, L.M.; Iana, G. Hydrogen Economy of the Fuel Cell Hybrid Power System optimized by air flow control to mitigate the effect of the uncertainty about available renewable power and load dynamics. *Energy Convers. Manag.* **2019**, *179*, 152–165. [[CrossRef](#)]
72. Bizon, N.; Lopez-Guede, J.M.; Hoarca, I.C.; Culcer, M.; Iliescu, M. Fuel Cell (FC) Hybrid Power System with mitigation of the load power variability by the FC fuel flow control information. In Proceedings of the International Conference on Electronics, Computers and Artificial Intelligence, Iasi, Romania, 27–30 June 2018.
73. Bizon, N. On tracking robustness in adaptive extremum seeking control of the fuel cell power plants. *Appl. Energy* **2010**, *87*, 3115–3130. [[CrossRef](#)]
74. Wang, L.; Chen, S.; Ma, K. On stability and application of extremum seeking control without steady-state oscillation. *Automatica* **2016**, *68*, 18–26. [[CrossRef](#)]
75. Bizon, N.; Thounthong, P.; Raducu, M.; Constantinescu, L.M. Designing and modelling of the asymptotic perturbed extremum seeking control scheme for tracking the global extreme. *Int. J. Hydrogen Energy* **2017**, *42*, 17632–17644. [[CrossRef](#)]
76. Oproescu, M.; Raducu, M.; Constantinescu, L.M.; Ramos-Hernanz, J.A.; Lopez-Guede, J.M. Evaluation of the performance of new extremum seeking control algorithm to locate accurately the peaks on multimodal functions. In Proceedings of the 2016 8th International Conference on Electronics, Computers and Artificial Intelligence (ECAI), Ploiesti, Romania, 30 June–2 July 2016. [[CrossRef](#)]
77. Secanell, M.; Wishart, J.; Dobson, P. Computational design and optimization of fuel cells and fuel cell systems: A review. *J. Power Sources* **2011**, *196*, 3690–3704. [[CrossRef](#)]
78. Yeniay, O. Penalty function methods for constrained optimization with genetic algorithms. *Math. Comput. Appl.* **2005**, *10*, 45–56. [[CrossRef](#)]
79. Kim, M.-J.; Peng, H. Power Management and Design Optimization of Fuel Cell/Battery Hybrid Vehicles. *J. Power Sources* **2007**, *165*, 819–832. [[CrossRef](#)]
80. Bizon, N.; Thounthong, P. Real-time strategies to optimize the fueling of the fuel cell hybrid power source: A review of issues, challenges and a new approach. *Renew. Sustain. Energy Rev.* **2018**, *91*, 1089–1102. [[CrossRef](#)]
81. Mumtaz, S.; Ali, S.; Ahmad, S.; Khan, L.; Hassan, S.Z.; Kamal, T. Energy Management and Control of Plug-In Hybrid Electric Vehicle Charging Stations in a Grid-Connected Hybrid Power System. *Energies* **2017**, *10*, 1923. [[CrossRef](#)]
82. Bizon, N.; Radut, M.; Oproescu, M. Energy control strategies for the Fuel Cell Hybrid Power Source under unknown load profile. *Energy* **2015**, *86*, 31–41. [[CrossRef](#)]
83. Wang, F.C.; Hsiao, Y.S.; Yang, Y.Z. The Optimization of Hybrid Power Systems with Renewable Energy and Hydrogen Generation. *Energies* **2018**, *11*, 1948. [[CrossRef](#)]
84. Bizon, N.; Mazare, A.G.; Ionescu, L.M.; Enescu, F.M. Optimization of the Proton Exchange Membrane Fuel Cell Hybrid Power System for Residential Buildings. *Energy Convers. Manag.* **2018**, *163*, 22–37. [[CrossRef](#)]
85. Bizon, N. Optimal Operation of Fuel Cell/Wind Turbine Hybrid Power System under Turbulent Wind and Variable Load. *Appl. Energy* **2018**, *212*, 196–209. [[CrossRef](#)]
86. Ahmadi, S.; Bathaee, S.M.T.; Hosseinpour, A.H. Improving fuel economy and performance of a fuel-cell hybrid electric vehicle (fuel-cell, battery, and ultra-capacitor) using optimized energy management strategy. *Energy Convers. Manag.* **2018**, *160*, 74–84. [[CrossRef](#)]
87. Tribioli, L.; Cozzolino, R. Techno-economic analysis of a stand-alone microgrid for a commercial building in eight different climate zones. *Energy Convers. Manag.* **2019**, *179*, 58–71. [[CrossRef](#)]

88. Hu, Z.; Li, J.; Xu, L.; Song, Z.; Fang, C.; Ouyang, M.; Dou, G.; Kou, G. Multi-objective energy management optimization and parameter sizing for proton exchange membrane hybrid fuel cell vehicles. *Energy Convers. Manag.* **2016**, *129*, 108–121. [CrossRef]
89. Bizon, N. Real-time optimization strategy for fuel cell hybrid power sources with load-following control of the fuel or air flow. *Energy Convers. Manag.* **2018**, *157*, 13–27. [CrossRef]
90. NASA. Technology Roadmaps—TA 3: Space Power and Energy Storage. 2015. Available online: https://www.nasa.gov/sites/default/files/atoms/files/2015_nasa_technology_roadmaps_ta_3_space_power_energy_storage_final.pdf (accessed on 18 December 2018).
91. Bizon, N.; Thounthong, P. Fuel Economy using the Global Optimization of the Fuel Cell Hybrid Power Systems. *Energy Convers. Manag.* **2018**, *173*, 665–678. [CrossRef]
92. Tan, Y.; Nešić, D.; Mareels, I. On non-local stability properties of extremum seeking control. *Automatica* **2006**, *42*, 889–903. [CrossRef]
93. Tan, Y.; Nešić, D.; Mareels, I.; Astolfi, A. On global extremum seeking in the presence of local extrema. *Automatica* **2009**, *45*, 245–251. [CrossRef]
94. Moura, S.J.; Chang, Y.A. Lyapunov-based switched extremum seeking for photovoltaic power maximization. *Control Eng. Pract.* **2013**, *21*, 971–980. [CrossRef]
95. Zhou, D.; Al-Durra, A.; Matraji, I.; Ravey, A.; Gao, F. Online Energy Management Strategy of Fuel Cell Hybrid Electric Vehicles: A Fractional-Order Extremum Seeking Method. *IEEE Trans. Ind. Electron.* **2018**, *65*, 6787–6799. [CrossRef]
96. Bizon, N.; Oproescu, M.; Raceanu, M. Efficient Energy Control Strategies for a Standalone Renewable/Fuel Cell Hybrid Power Source. *Energy Convers. Manag.* **2015**, *90*, 93–110. [CrossRef]
97. Bizon, N.; Culcer, M.; Iliescu, M.; Mazare, A.G.; Ionescu, L.M.; Beloiu, R. Real-time strategy to optimize the Fuel Flow rate of Fuel Cell Hybrid Power Source under variable load cycle. In Proceedings of the International Conference on Electronics, Computers and Artificial Intelligence, Targoviste, Romania, 29 June–1 July 2017. [CrossRef]
98. Bizon, N.; Culcer, M.; Oproescu, M.; Iana, G.; Ionescu, L.M.; Mazare, A.G.; Iliescu, M. Real-time strategy to optimize the Airflow rate of Fuel Cell Hybrid Power Source under variable load cycle. In Proceedings of the 22rd International Conference on Applied Electronics—APPEL 2017, Pilsen, Czech Republic, 5–7 September 2017. [CrossRef]
99. Bizon, N. Energy optimization of Fuel Cell System by using Global Extremum Seeking algorithm. *Appl. Energy* **2017**, *206*, 458–474. [CrossRef]
100. Erdinç, O.; Vural, B.; Uzunoglu, M. A wavelet-fuzzy logic based energy management strategy for a fuel cell/battery/ultra-capacitor hybrid vehicular power system. *J. Power Sources* **2009**, *194*, 369–380. [CrossRef]
101. Sulaiman, N.; Hannan, M.A.; Mohamed, A.; Ker, P.J.; Majlan, E.H.; Wan Daud, W.R. Optimization of energy management system for fuel-cell hybrid electric vehicles: Issues and recommendations. *Appl. Energy* **2018**, *228*, 2061–2079. [CrossRef]
102. Nikiforow, K.; Koski, P.; Ihonen, J. Discrete ejector control solution design, characterization, and verification in a 5 kW PEMFC system. *Int. J. Hydrogen Energy* **2017**, *42*, 16760–16772. [CrossRef]
103. Bizon, N. Effective Mitigation of the Load Pulses by Controlling the Battery/SMES Hybrid Energy Storage System. *Appl. Energy* **2018**, *229*, 459–473. [CrossRef]

